Cell Reports

Drosophila CLASP regulates microtubule orientation and dendrite pruning by suppressing Par-1 kinase

Graphical abstract

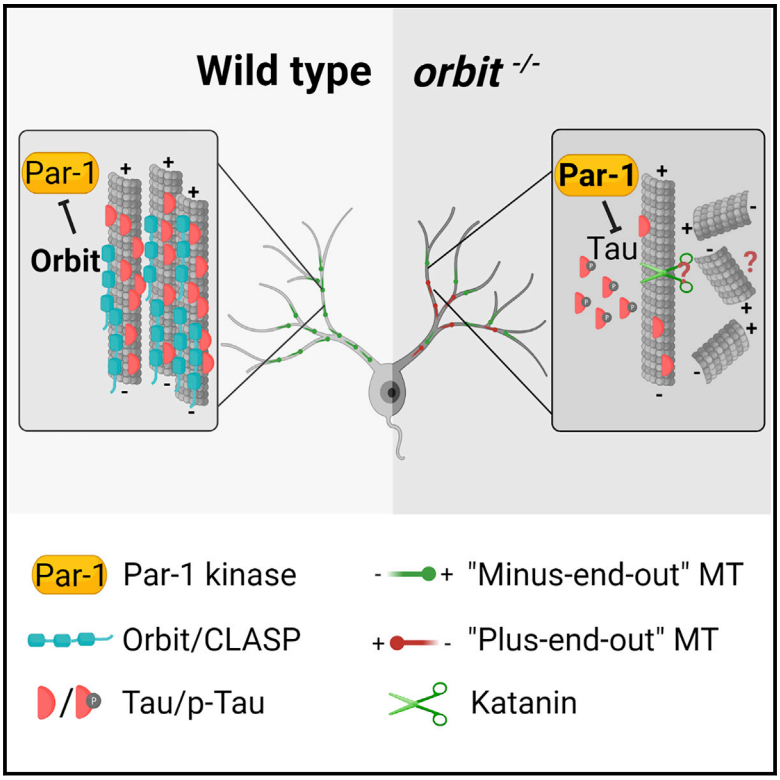

Highlights

- The *Drosophila* CLASP homolog Orbit regulates dendrite pruning of sensory neurons
- Orbit maintains the minus-end-out microtubule orientation in dendrites
- Par-1 kinase is a genetic suppressor of Orbit in dendritic microtubule orientation
- Gain of Par-1 function phenocopies *orbit* mutants

Authors

Shufeng Bu, Quan Tang, Yan Wang, Samuel Song Yuan Lau, Wei Lin Yong, Fengwei Yu

Correspondence

fengwei@tll.org.sg

In brief

Bu et al. report a key role of *Drosophila* CLASP in regulating neuronal pruning of ddaC sensory neurons during development. Orbit is required for maintenance of the minus-end-out microtubule orientation in the dendrites. Importantly, *Drosophila* CLASP governs dendritic microtubule orientation and dendrite pruning at least partly via suppressing Par-1 kinase.

Bu et al., 2022, Cell Reports *39*, 110887
May 31, 2022
https://doi.org/10.1016/j.celrep.2022.110887

CellPress

Cell Reports

CellPress
OPEN ACCESS

Report

Drosophila CLASP regulates microtubule orientation and dendrite pruning by suppressing Par-1 kinase

Shufeng Bu,[1,2] Quan Tang,[1] Yan Wang,[1] Samuel Song Yuan Lau,[1] Wei Lin Yong,[1] and Fengwei Yu[1,2,3,*]
[1]Temasek Life Sciences Laboratory, 1 Research Link, National University of Singapore, Singapore, Singapore
[2]Department of Biological Sciences, National University of Singapore, Singapore, Singapore
[3]Lead contact
*Correspondence: fengwei@tll.org.sg
https://doi.org/10.1016/j.celrep.2022.110887

SUMMARY

The evolutionarily conserved CLASPs (cytoplasmic linker-associated proteins) are microtubule-associated proteins that inhibit microtubule catastrophe and promote rescue. CLASPs can regulate axonal elongation and dendrite branching in growing neurons. However, their roles in microtubule orientation and neurite pruning in remodeling neurons remain unknown. Here, we identify the *Drosophila* CLASP homolog Orbit/MAST, which is required for dendrite pruning in ddaC sensory neurons during metamorphosis. Orbit is important for maintenance of the minus-end-out microtubule orientation in ddaC dendrites. Our structural analysis reveals that the microtubule lattice-binding TOG2 domain is required for Orbit to regulate dendritic microtubule orientation and dendrite pruning. In a genetic modifier screen, we further identify the conserved Par-1 kinase as a suppressor of Orbit in dendritic microtubule orientation. Moreover, elevated Par-1 function impairs dendritic microtubule orientation and dendrite pruning, phenocopying *orbit* mutants. Overall, our study demonstrates that *Drosophila* CLASP governs dendritic microtubule orientation and dendrite pruning at least partly via suppressing Par-1 kinase.

INTRODUCTION

Selective elimination of unnecessary or exuberant neurites without loss of parental neurons, also known as pruning, is a crucial step for the maturation of the nervous system during animal development (Luo and O'Leary, 2005; Riccomagno and Kolodkin, 2015; Schuldiner and Yaron, 2015). The *Drosophila* dendrite arborization (da) sensory neurons have emerged as an important *in vivo* model to study molecular mechanisms of neuronal pruning during metamorphosis, a transition stage between larval and adult stages (Yu and Schuldiner, 2014). Pruning of the nervous system is triggered by an impulse of the steroid hormone ecdysone at the late larval stage (Truman, 1990). A subset of dorsal da neurons, such as ddaC (class IV, also known as C4da) neurons, selectively prune away their dendrites without affecting their axons (Kuo et al., 2005; Shimono et al., 2009; Williams and Truman, 2005). In ddaC neurons, the proximal dendrites undergo severing at 5–8 h after puparium formation (APF), followed by dendrite fragmentation and clearance by 16 h APF (Han et al., 2014; Williams and Truman, 2005). During dendrite pruning, local microtubule disassembly at the proximal dendrites precedes dendritic membrane breakage (Lee et al., 2009; Williams and Truman, 2005). Several negative regulators of microtubules, including Par-1 kinase, Katanin p60-like 1 (Kat-60L1), Efa6, and Stathmin, have been reported to promote dendrite pruning possibly via triggering local microtubule disassembly (Bu et al., 2021; Herzmann et al., 2017; Lee et al., 2009; Sun et al., 2021).

Microtubules are polarized filaments that consist of α, β-tubulins. The β-tubulin-exposing plus ends undergo fast growth and shrinkage, while the α-tubulin-exposing minus ends are more stable (Akhmanova and Steinmetz, 2008). In mature mammalian neurons, axonal microtubules are uniformly aligned with their plus ends distal to the soma (plus-end-out), whereas dendritic microtubules are arranged in a mixed orientation (Akhmanova and Steinmetz, 2015; Baas and Lin, 2011). In fly and worm neurons, axonal microtubules are oriented plus-end-out, similar to those in mammalian ones. However, microtubules in the major dendrites are predominantly arranged with their minus ends distal to the soma (minus-end-out) (Goodwin et al., 2012; Ori-McKenney et al., 2012; Stone et al., 2008; Yan et al., 2013). We and others previously reported that depletion of microtubule-associated proteins (MAPs) or kinesin motors disrupts the minus-end-out microtubule orientation in the dendrites and thereby impairs dendrite pruning in ddaC neurons (Feng et al., 2019; Herzmann et al., 2018; Rui et al., 2020; Tang et al., 2020; Wang et al., 2019). However, it is still unclear how the minus-end-out microtubule orientation is maintained in the dendrites.

Drosophila Orbit/MAST belongs to the CLASP (cytoplasmic linker-associated protein) family of MAPs that can function as microtubule plus-end-tracking proteins, protect microtubules from catastrophe, and promote rescue (Al-Bassam and Chang,

2011; Lawrence et al., 2020). In mammals, there are two paralogs of Orbit/CLASP proteins, including a ubiquitously expressed CLASP1 and a brain-specific CLASP2 (Akhmanova et al., 2001), whereas the *Drosophila* genome encodes only one *CLASP* gene, namely, *orbit/mast* (Inoue et al., 2000; Lemos et al., 2000). Loss of *orbit/mast* function in mitotic cells leads to defects in kinetochore-microtubule attachment, chromosome condensation, and spindle bipolarity (Lemos et al., 2000; Maiato et al., 2002). Neuronal Orbit/CLASP proteins are enriched in the growth cones during neurite outgrowth stage (Beffert et al., 2012; Hur et al., 2011; Lee et al., 2004). In cultured mammalian neurons, loss of CLASP2 results in impaired axonal growth and dendritic branching, while overexpression of CLASP2 causes multiple axonal initiation and dendrite overgrowth (Beffert et al., 2012; Hur et al., 2011). However, the roles of Orbit and its mammalian orthologs CLASPs in regulating neuronal microtubule orientation and neuronal pruning remain unknown. Here, we report important roles of the *Drosophila* CLASP protein Orbit in regulating dendrite pruning and microtubule orientation in remodeling neurons.

RESULTS

Orbit/MAST is required for dendrite pruning of sensory neurons

In a MARCM (mosaic analysis with a repressible cell marker) screen, we isolated a mutant line, *l(3L)464*, which exhibited prominent dendrite severing defects in most of the ddaC neurons at 16 h APF (Figures 1D, 1J, and 1K). By contrast, the control clones eliminated their dendritic branches (Figures 1C, 1J, and 1K). In addition, initial da was affected in *l(3L)464* mutant clones at the wandering third instar larval (wL3) stage (Figure S1A). We then mapped this mutation to the cytological region 78C2 (Figure 1A). Moreover, it failed to complement with two previously published *orbit* alleles, $orbit^{3}$ and $orbit^{4}$ (Inoue et al., 2000). Therefore, we named *l(3L)464* as $orbit^{464}$ allele thereafter.

We further confirmed the important role of *orbit* in dendrite pruning. First, like $orbit^{464}$, either $orbit^{4}$ or $orbit^{3}$ mutant clones showed consistent dendrite pruning defects with similar penetrance (Figures 1F and 1I–1K). Second, we carried out several rescue experiments in $orbit^{464}$ or $orbit^{4}$ mutants by expressing *orbit* transgenes containing its genomic fragments, *g-orbit* (also known as *pB14*) (Inoue et al., 2000) and *g-orbit-tdGFP* (Figure 1B). Either *g-orbit* or *g-orbit-tdGFP* genomic transgenes rescued both lethality and dendrite pruning phenotypes associated with $orbit^{464}$ or $orbit^{4}$ mutants (Figures 1E, 1G, 1H, 1J, and 1K). Finally, *ppk-Gal4*-driven expression of two independent *orbit* RNAi lines (#1, BL35442; #2, v106820) in ddaC neurons also caused consistent dendrite pruning defects (Figure S1B). Thus, Orbit is cell autonomously required for dendrite pruning of ddaC neurons.

We next examined the expression and localization of Orbit by using either *g-orbit-tdGFP* or *UASp-GFP-Orbit* transgenes. Both GFP-fused Orbit proteins are functional and can substitute for the endogenous Orbit protein, because their expression largely rescued the dendrite pruning defects in $orbit^{4}$ mutant neurons (Figures 1H and S3C). Using the *g-orbit-tdGFP* genomic transgene, we observed the expression of Orbit in ddaC neurons and the surrounding epidermal cells (Figure S1C). Both GFP-fused Orbit proteins largely co-localized with α-tubulin on the microtubule lattices in these cells (Figures S1C and S1D).

Overexpression of orbit inhibits dendrite pruning

To investigate its potential gain-of-function effect, we generated both untagged and tagged *orbit* transgenes under the control of the *UASt* promoter. Interestingly, overexpression of Orbit or Orbit-CTAP caused severe dendrite pruning defects in the vast majority of ddaC neurons, compared with the control (Figure S2A). Moreover, initial da was strongly impaired in Orbit-overexpressing neurons at the white prepupal (WP) stage (Figure S2A). To rule out the possibility that the dendrite pruning defects are caused by initial da defects, we used the Gene-Switch system to temporally induce the expression of Orbit at the third instar larval stage. After 1-day RU486 treatment, the GeneSwitch-Gal4-driven expression of Orbit-GFP did not affect the number of major dendrites at WP stage (Figure S2B). Importantly, 90% of Orbit-GFP-expressing ddaC neurons also displayed dendrite severing defects (Figure S2B). Collectively, our data suggest that dendrite pruning of ddaC neurons requires precise control of Orbit protein level.

The TOG2 domain is important for orbit to regulate dendrite pruning

Drosophila Orbit and its mammalian homologs CLASPs share the same domain architecture, namely, three TOG or TOG-like domains that can bind to tubulin dimers, an EB1-binding SxIP motif that can target CLASPs to the plus ends, and a C-terminal CLIP-interacting domain (CLIP-ID) (Figure S3A) (Aher et al., 2018; Honnappa et al., 2009; Leano et al., 2013). To investigate which protein domains of Orbit are important for its function in dendrite pruning, we generated a series of transgenes that express various truncated Orbit proteins under the germline *UASp* promoter (Figure S3A). The *UASp-Orbit* transgene induced extremely low-level expression of the protein in ddaC neurons, compared with those *UASt* transgenes (Figure S2C). As controls, *UASp*-dependent expression of Orbit and its variants resulted in no or very mild dendrite pruning defects in ddaC neurons at 16 h APF (data not shown), compared with high-level expression of Orbit. The expression of the full-length Orbit protein ($Orbit^{FL}$) almost fully rescued the dendrite pruning defects in $orbit^{4}$ ddaC neurons (Figures S3D, S3L, and S3M), compared with the $orbit^{4}$ control alone (Figure S3B). Interestingly, $Orbit^{\Delta TOG1}$ (Figure S3E), $Orbit^{\Delta SxIP}$ (Figure S3G), $Orbit^{\Delta TOG3}$ (Figure S3H), $Orbit^{\Delta CLIP\text{-}ID}$ (Figure S3I), or $Orbit^{TOG1,2-linker}$ (Figure S3J) deletion constructs fully or largely rescued the dendrite pruning defects in $orbit^{4}$ mutant clones (Figures S3L and S3M), suggesting that TOG1, SxIP, TOG3, and CLIP-ID are dispensable for Orbit's function in dendrite pruning. We further tested the importance of the TOG2 domain of Orbit during dendrite pruning. Indeed, the $Orbit^{\Delta TOG2}$ variant failed to rescue the pruning phenotype of $orbit^{4}$ mutant neurons (Figure S3F). Moreover, the TOG2 domain alone significantly suppressed the $orbit^{4}$ mutant phenotype (Figures S3K–S3M). Thus, the TOG2 domain is important for Orbit to regulate dendrite pruning in ddaC neurons.

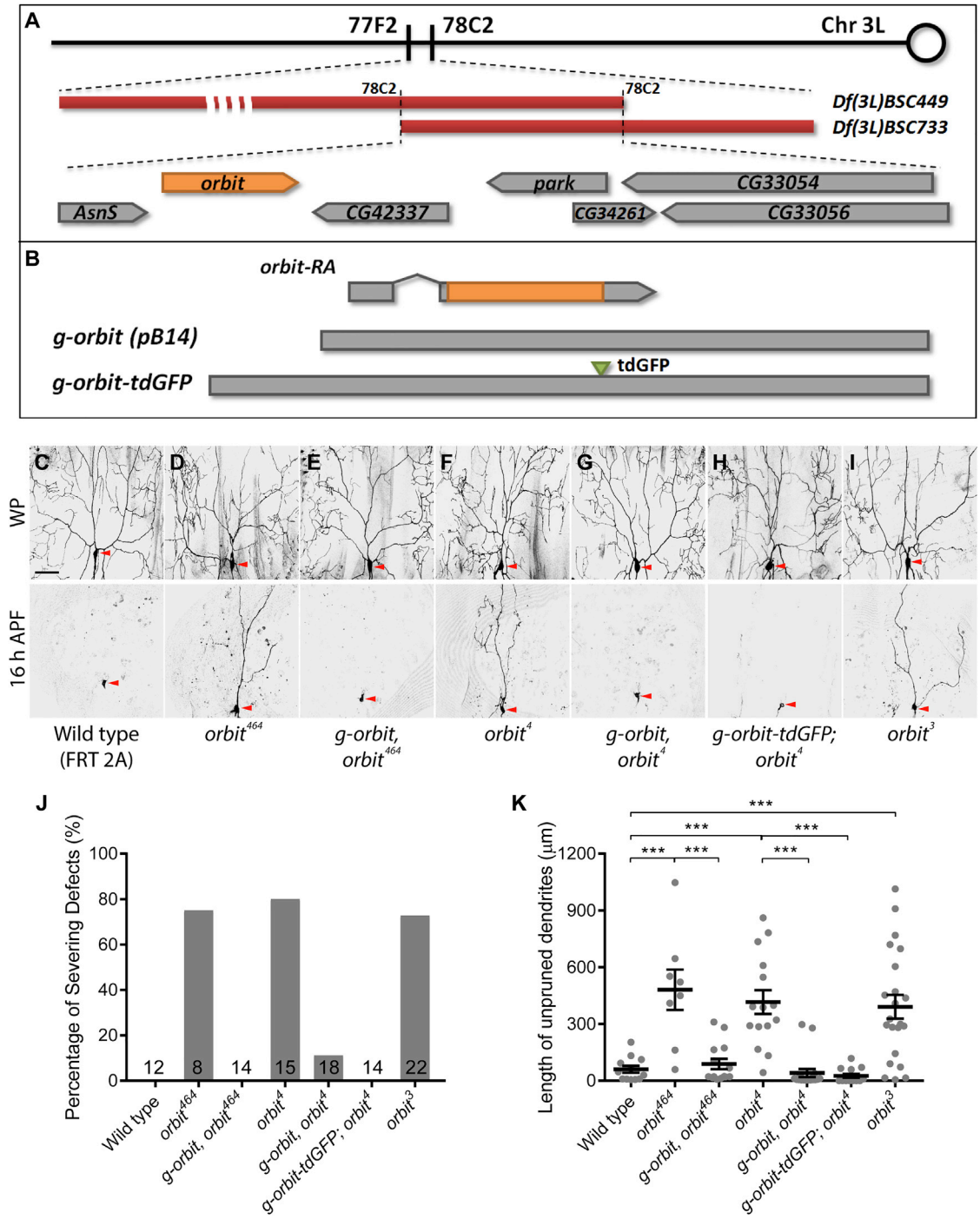

Figure 1. Orbit/MAST is required for dendrite pruning of sensory neurons

(A) Location of *Drosophila orbit* gene (orange) on chromosome 3 left arm. *l(3L)464* mutant allele failed to complement with *Df(3L)BSC499* and *Df(3L)BSC733* (red).

(B) A diagram of *orbit* gene structure and genomic rescue constructs, *g-orbit* and *g-orbit-tdGFP*. The coding region of *orbit* is highlighted in orange.

(C–I) Dendrites of wild type (C), $orbit^{464}$ (D), *g-orbit,* $orbit^{464}$ (E), $orbit^{4}$ (F), *g-orbit,* $orbit^{4}$ (G), *g-orbit-tdGFP;* $orbit^{4}$ (H), or $orbit^{3}$ (I) ddaC neurons at WP and 16 h APF. Red arrowheads point to the soma of ddaC (biological replicates >5).

(J and K) Quantitative analyses of dendrite severing defects and unpruned dendrite length at 16 h APF.

The error bars represent SEM. The scale bar in (C) represents 50 μm. ***$p < 0.001$. See also Figures S1–S3 and Table S1.

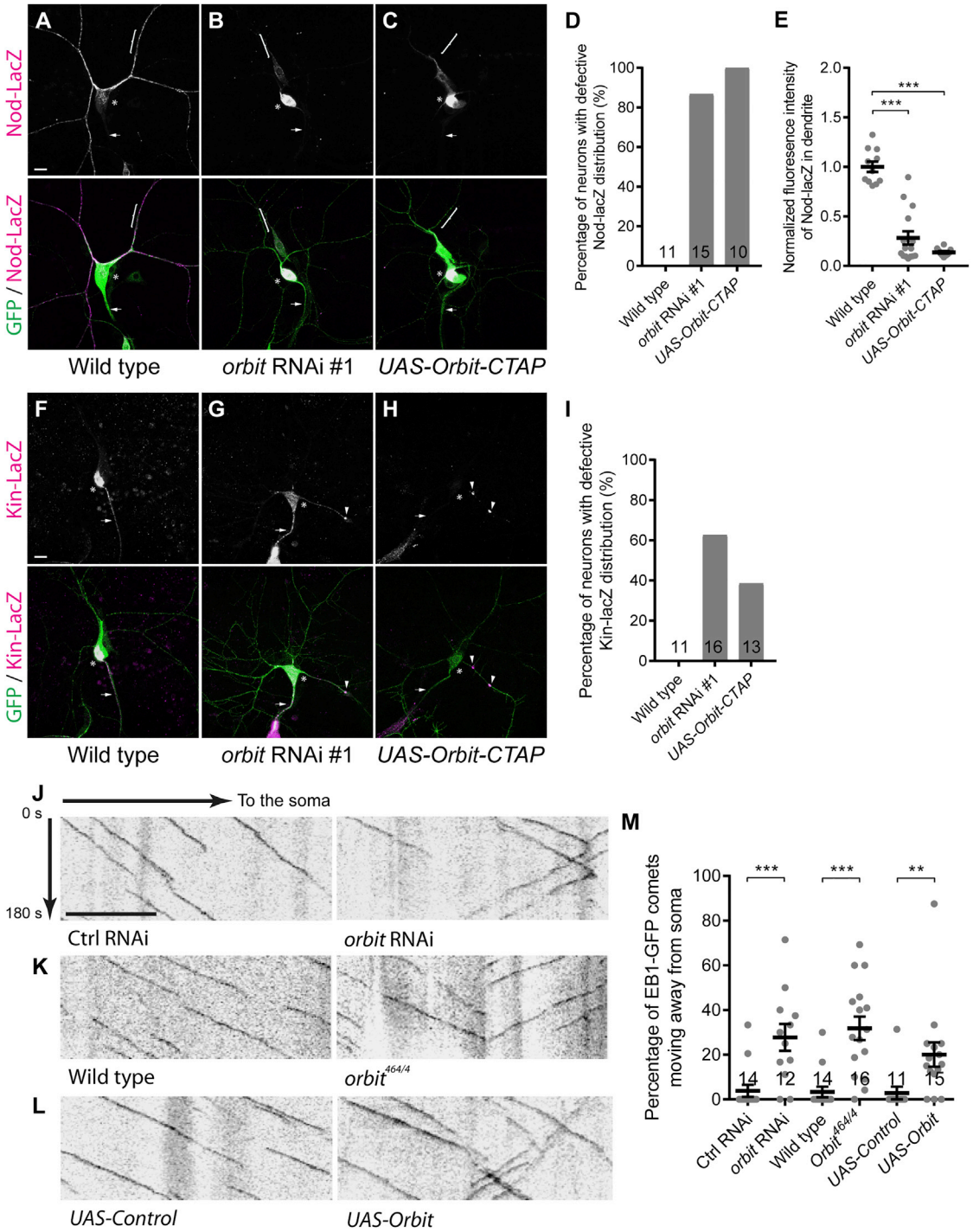

Figure 2. Orbit is required for the minus-end-out microtubule orientation in the dendrites of ddaC neurons

(A–C) Expression of Nod-lacZ (magenta) in ddaC neurons (green) of wild-type (A), *orbit* RNAi #1 (B), or Orbit-CTAP overexpression (C). The asterisks label the ddaC somas, the arrows point to the axons, and the brackets mark the dendrites (biological replicates = 3).

(D and E) Quantitative analysis of Nod-lacZ distribution in the ddaC dendrites.

(F–H) Expression of Kin-lacZ (magenta) in ddaC neurons (green) of wild-type (F), *orbit* RNAi #1 (G), or Orbit-CTAP overexpression (H). The asterisks label the ddaC somas, the arrows point to the axons, and the arrowheads point to the dendrites where Kin-lacZ is accumulated (biological replicates = 3).

(legend continued on next page)

Orbit regulates dendritic microtubule stability and turnover in the dendrites of ddaC neurons

We next assessed whether Orbit regulates microtubule stability and turnover in ddaC neurons. Using Futsch/22C10 as a microtubule marker (Roos et al., 2000), we found that dendritic microtubule levels were strongly reduced in *orbit* RNAi neurons but significantly elevated in Orbit-overexpressing ddaC neurons at the wL3 stage (Figure S4A). These data indicate that Orbit can stabilize dendritic microtubules in postmitotic ddaC neurons. To test whether Orbit is important for microtubule turnover in the dendrites, we conducted the photoconversion assays by expressing a photoconvertible tdEOS:α-tubulin (Barlan et al., 2013; Bu et al., 2021; Herzmann et al., 2017; Lu et al., 2013; Tao et al., 2016). Because mature neurons lose the ability of microtubule sliding (Lu et al., 2013, 2015), the photoconversion assays can be used to measure microtubule turnover or disassembly in ddaC neurons from the third instar larval stage (Tao et al., 2016). In the dendrites of orbit RNAi ddaC neurons, the amounts of the photoconverted tdEOS:α-tubulin remaining were significantly reduced at wL3, as compared with those in control neurons (Figure S4B), suggesting higher microtubule turnover on orbit knockdown. Overexpression of full-length Orbit, but not Orbit$^{\Delta TOG2}$, rescued the microtubule turnover defects in the dendrites of *orbit*$^{4/464}$ mutant neurons (Figure S4C), indicating that the TOG2 domain is required for Orbit to regulate microtubule turnover. Interestingly, the converted tdEOS:α-tubulin signals also decayed faster in Orbit-overexpressing neurons than those in the control neurons (Figure S4B), suggesting that microtubules in the dendrites of Orbit-overexpressing neurons, albeit increased in level (Figure S4A), are more dynamic. Thus, these data suggest that both reduction and overexpression of Orbit enhance microtubule turnover in dendrites. A previous study has reported that higher microtubule turnover can accelerate the dendrite pruning process in ddaC neurons, leading to precocious dendrite pruning at 7 h APF (Bu et al., 2021). Unexpectedly, our present data indicate that both loss and gain of *orbit* functions did not lead to precocious dendrite pruning but rather caused the dendrite pruning defects in ddaC neurons (Figures 1 and S2). Moreover, either *orbit* RNAi knockdown or overexpression resulted in increases in dendritic microtubule levels at 6 h APF (Figure S5A), suggesting that both *orbit* RNAi knockdown and overexpression lead to inhibition of microtubule disassembly before the onset of dendrite pruning. Taken together, our data suggest that Orbit does not regulate dendrite pruning by directly facilitating dendritic microtubule disassembly.

Orbit is required for the minus-end-out microtubule orientation in the dendrites of ddaC neurons

We next examined whether the dendritic microtubule orientation is impaired in *orbit* loss-of-function or gain-of-function neurons. To this end, we first detected the distribution of two microtubule markers, namely, Nod-LacZ and Kin-LacZ, in *orbit* RNAi or Orbit-overexpressing neurons. The chimera Nod-LacZ is often used as a marker of microtubule minus ends in *Drosophila* (Clark et al., 1997). Nod-LacZ was enriched in the dendrites but absent in the axons of wild-type ddaC neurons (Figure 2A). By contrast, Nod-LacZ was absent or significantly reduced in almost all the dendrites but strongly accumulated in the soma of *orbit* RNAi ddaC neurons (Figures 2B and 2D). Dendritic Nod-LacZ levels in *orbit* RNAi neurons were drastically reduced to 28% of those in the control neurons (Figure 2E). Similarly, overexpression of Orbit-CTAP also caused robust accumulation of Nod-LacZ signals in the soma with reduced dendritic distribution in all ddaC neurons (Figures 2C–2E), resembling the *orbit* RNAi phenotypes. The axon-specific marker Kin-LacZ is often used as a marker of microtubule plus ends (Clark et al., 1997). Kin-LacZ was localized in the axons, but not in the dendrites, of wild-type ddaC neurons (Figure 2F) (Zheng et al., 2008). Interestingly, Kin-LacZ often mis-localized as punctate structures in the dendrites of *orbit* RNAi (Figures 2G and 2I) or Orbit-CTAP-overexpressing ddaC neurons (Figures 2H and 2I). Thus, Orbit is important for proper distribution of dendrite or axon-specific microtubule markers in ddaC neurons.

Moreover, we made use of the microtubule plus-end marker EB1-GFP to determine the dendritic microtubule orientation (Rolls et al., 2007; Stepanova et al., 2003). In the major dendrites of control neurons, almost all the EB1-GFP comets moved toward the soma (retrograde) (Figure 2J), with only 4% of the comets migrating away from the soma (anterograde) (Figure 2M), suggesting a nearly uniform minus-end-out microtubule orientation in the mature dendrites (Mattie et al., 2010; Stone et al., 2008). Importantly, anterograde EB1-GFP comets were significantly increased to 28% in the dendrites of *orbit* RNAi neurons (Figures 2J and 2M). Likewise, a large proportion (32%) of dendritic EB1-GFP comets moved anterogradely in *orbit*$^{4/464}$ trans-heterozygous mutant neurons (Figures 2K and 2M). Similar to *orbit* mutants, Orbit-overexpressing neurons also exhibited 20% of EB1-GFP comets that migrated anterogradely in their major dendrites, compared with the control neurons (3%) (Figures 2L and 2M). Moreover, we also examined the domains of Orbit required for microtubule orientation in ddaC dendrites. Consistent with their abilities to rescue the dendrite pruning defects (Figures S3L and S3M), low-level expression of Orbit^{FL}, Orbit$^{TOG1,2-Linker}$, or Orbit$^{\Delta SxIP}$ was also able to fully rescue the microtubule orientation phenotypes in *orbit*$^{4/464}$ mutant ddaC neurons (Figure S5B). Importantly, Orbit^{TOG2}, but not Orbit$^{\Delta TOG2}$, significantly suppressed the dendritic microtubule orientation defect in *orbit*$^{4/464}$ mutant ddaC neurons (Figure S5B), as well as the dendrite pruning defects (Figures S3F and S3K–S3M). These structure-function analyses indicate that the TOG2 domain is important for the protein to govern the minus-end-out microtubule orientation in the dendrites and thereby facilitate dendrite pruning in ddaC neurons.

(I) Quantitative analysis of Kin-lacZ distribution in the ddaC dendrites.
(J–L) Dendritic EB1-GFP kymographs in *orbit* RNAi (J), *orbit*$^{464/4}$ mutant (K), or Orbit-overexpressing (L) ddaC neurons with their respective controls. The horizontal arrow marks the direction toward the soma. The vertical arrow indicates the duration (biological replicates >3).
(M) Quantitative analysis of EB1-GFP orientation in the ddaC dendrites.
The error bars represent SEM. The scale bars in (A), (F), and (J) represent 10 μm. **p < 0.01, ***p < 0.001. See also Figures S4 and S5 and Table S1.

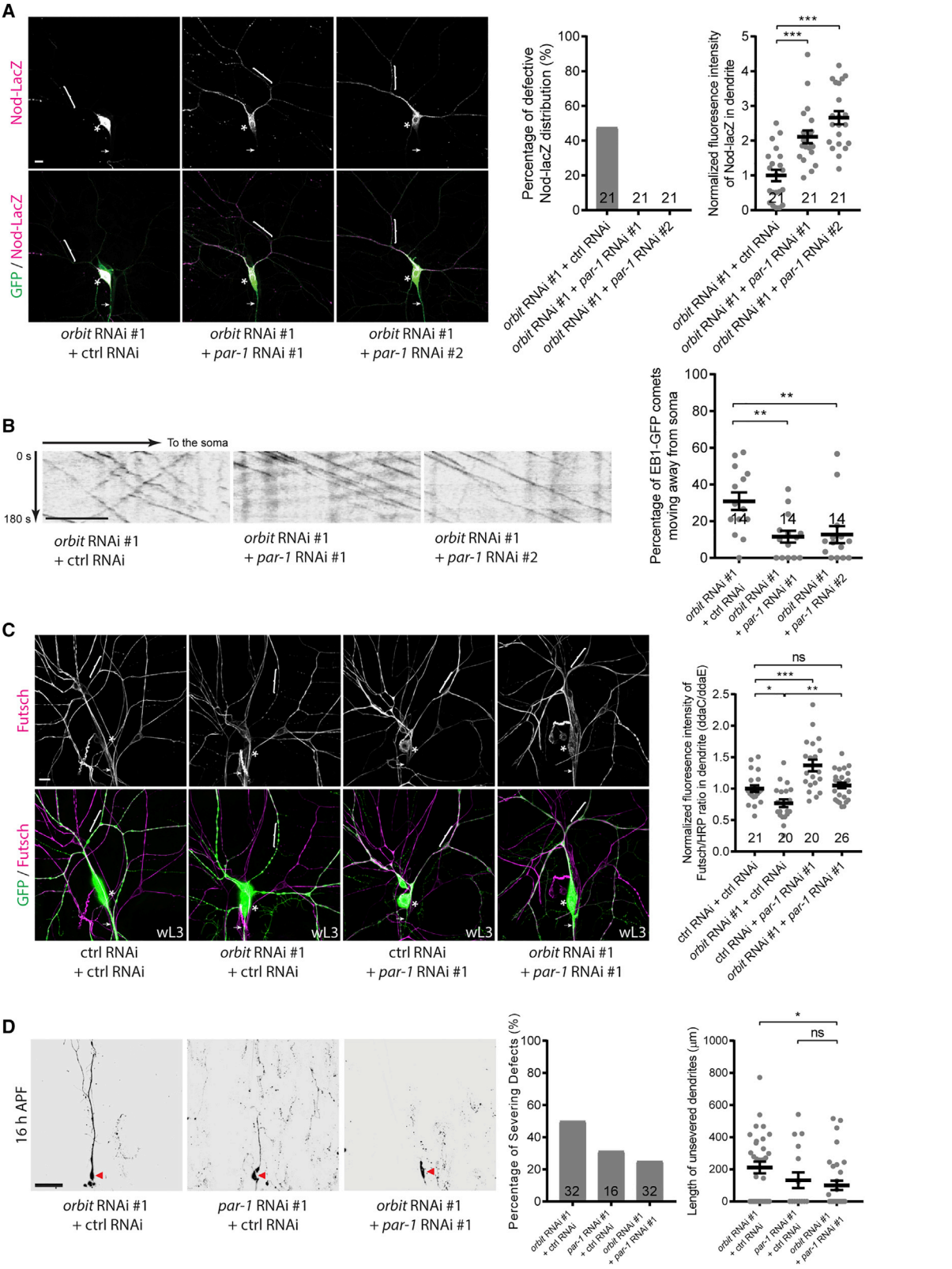

(legend on next page)

A genetic modifier screen identifies Par-1 kinase as a suppressor of orbit in regulating dendritic microtubule orientation

Orbit and CLASPs interact with CLIP proteins in flies and mammals (Akhmanova et al., 2001; Mathe et al., 2003). However, CLIP-ID of Orbit is dispensable for dendrite pruning (Figures S3I, S3L, and S3M). Moreover, *clip-190* null mutant (*clip-190*^{KO}) and RNAi lines did not show any dendrite pruning defects in ddaC neurons (data not shown). Mammalian CLASPs have also been reported to interact with the Golgi protein GCC185 to promote noncentrosomal microtubule nucleation at the *trans*-Golgi network (Efimov et al., 2007). However, knockdown of GCC185 with two RNAi lines did not cause dendrite pruning defects in ddaC neurons (data not shown); Orbit did not form a protein complex with fly GCC185 in transfected S2 cells in the co-immunoprecipitation assays (Figure S5C). Thus, Orbit unlikely regulates dendrite pruning via CLIP-190 or GCC185.

To understand the mechanism whereby Orbit regulates dendritic microtubule orientation, we conducted a genetic modifier screen using Nod-LacZ as a readout of dendritic microtubule orientation. Interestingly, among various RNAi lines targeting 21 microtubule regulators (see STAR Methods), we isolated two independent RNAi lines targeting Par-1 kinase (#1, BL#32410; #2, BL#35342) that fully rescued the Nod-LacZ localization defects in *orbit* RNAi neurons (Figure 3A). As a control, RNAi knockdown of Par-1 (#1 or #2) alone did not affect the Nod-lacZ distribution in ddaC dendrites (Figure S6A). Par-1, also known as microtubule affinity-regulating kinase (MARK) in mammals, acts as a negative microtubule regulator that can phosphorylate MAPs (such as Tau) to destabilize microtubules (Drewes et al., 1997; Guo and Kemphues, 1995; Nishimura et al., 2004). We then conducted the EB1-GFP assays to strengthen the Nod-LacZ results. Knockdown of *par-1* (#1 or #2) did not affect the minus-end-out microtubule orientation in the dendrites; however, the number of dendritic EB1-GFP comets was significantly increased (Figure S6B). Importantly, when either of the *par-1* RNAi constructs was expressed in *orbit* RNAi mutant neurons, the dendritic microtubule orientation defects were suppressed, because the proportion of anterograde EB1-GFP comets was significantly decreased from 31% to 12% (*par-1* RNAi #1) or 13% (*par-1* RNAi #2) (Figure 3B). The antagonism between Orbit and Par-1 is specific, because knockdown of the microtubule depolymerizing kinesin Klp10A, via either of two functional RNAi lines (Wang et al., 2019), did not rescue the defects in Nod-LacZ distribution or EB1-GFP directionality in *orbit* RNAi neurons (Figures S7A and S7B). Klp10A has been shown to depolymerize microtubules from both minus and plus ends (Goodwin and Vale, 2010; Mennella et al., 2005). Moreover, attenuation of Klp10A is able to restore the minus-end-out microtubule orientation in the dendrites of *patronin* or *mini-spindles* (*msps*) mutant neurons (Tang et al., 2020; Wang et al., 2019). Thus, Orbit unlikely acts on microtubule ends to regulate the dendritic microtubule orientation.

Futsch levels in the dendrites of *par-1* RNAi neurons were significantly increased (Figure S6C), consistent with a previous study (Herzmann et al., 2017). Interestingly, knockdown of Par-1 also restored normal Futsch levels in the dendrites of *orbit* RNAi neurons (Figure 3C), compared with those in control RNAi neurons. Thus, our findings suggest that Orbit functions to govern dendritic minus-end-out orientation and microtubule levels at least partly via suppressing Par-1 function.

Consistent with the previous finding (Herzmann et al., 2017), we also found that 17% of ddaC neurons expressing the *par-1* RNAi (#1) construct exhibited the dendrite severing defects at 16 h APF (Figure S6D). Interestingly, further knockdown of *par-1* did not enhance but significantly suppressed the dendrite pruning defects in *orbit* RNAi ddaC neurons (Figure 3D). The dendrite pruning defects associated with *par-1* and *orbit* double RNAi knockdown largely resembled the *par-1* RNAi phenotype alone (Figure 3D). Thus, these data suggest that *par-1* is epistatic to *orbit* in dendrite pruning.

Par-1 overexpression impairs dendritic microtubule orientation and dendrite pruning

Our genetic suppression data suggest that Orbit and Par-1 play an antagonistic role in dendritic microtubule orientation and dendrite pruning. We then asked whether Par-1 overexpression phenocopies loss/knockdown of *orbit* function. Indeed, overexpression of wild-type Par-1 (Par-1^{WT}) led to dramatic accumulation of Nod-LacZ signals in the soma with significant reduction in the dendrites (Figure 4A). Consistently, overexpression of Par-1^{WT} significantly increased the proportion of anterograde dendritic EB1-GFP comets to 11%, compared with 1% in the control neurons (Figure 4B). Par-1 overexpression also caused the dendrite severing defects in 38% of ddaC neurons (Figure 4C). Thus, Par-1 overexpression resembles the effects of loss/reduction of *orbit* function.

Figure 3. Orbit regulates microtubule orientation in ddaC dendrites via antagonizing Par-1 function

(A) Expression of Nod-lacZ (magenta) in *orbit* RNAi #1 ddaC neurons (green) co-expressing control [ctrl] RNAi, *par-1* RNAi #1, or *par-1* RNAi #2 construct. The asterisks label the ddaC somas, the arrows point to the axons, and the brackets mark the dendrites (biological replicates = 5). Quantitative analysis of Nod-lacZ distribution in the ddaC dendrites.

(B) Dendritic EB1-GFP kymographs in *orbit* RNAi #1 + ctrl RNAi, *orbit* RNAi #1 + *par-1* RNAi #1, and *orbit* RNAi #1 + *par-1* RNAi #2 ddaC neurons. The horizontal arrow marks the direction toward the soma (biological replicates >3), and the vertical arrow indicates the duration. Quantitative analysis of EB1-GFP orientation in the dendrites.

(C) Microtubule/Futsch (magenta) levels in ddaC neurons (green) expressing two copies of ctrl RNAi, *orbit* RNAi #1 + ctrl RNAi, ctrl RNAi + *par-1* RNA #1, or *orbit* RNAi #1 + *par-1* RNAi #1. The asterisks label the ddaC somas, the arrows point to the axons, and the brackets mark the dendrites (biological replicates = 5). Quantitative analysis of microtubule levels in the ddaC dendrites.

(D) Dendrites of ddaC neurons co-expressing *orbit* RNAi #1 + ctrl RNAi, *par-1* RNAi #1 + ctrl RNAi, or *orbit* RNAi #1 + *par-1* RNAi #1 constructs at 16 h APF. Red arrowheads point to the soma of ddaC (biological replicates >5). Quantitative analyses of dendrite severing defects and unsevered dendrite length.

The error bars represent SEM. Scale bars represent 10 μm (A–C) and 50 μm (D). *p < 0.05, **p < 0.01, ***p < 0.001. ns, not significant. See also Figures S6 and S7 and Table S1.

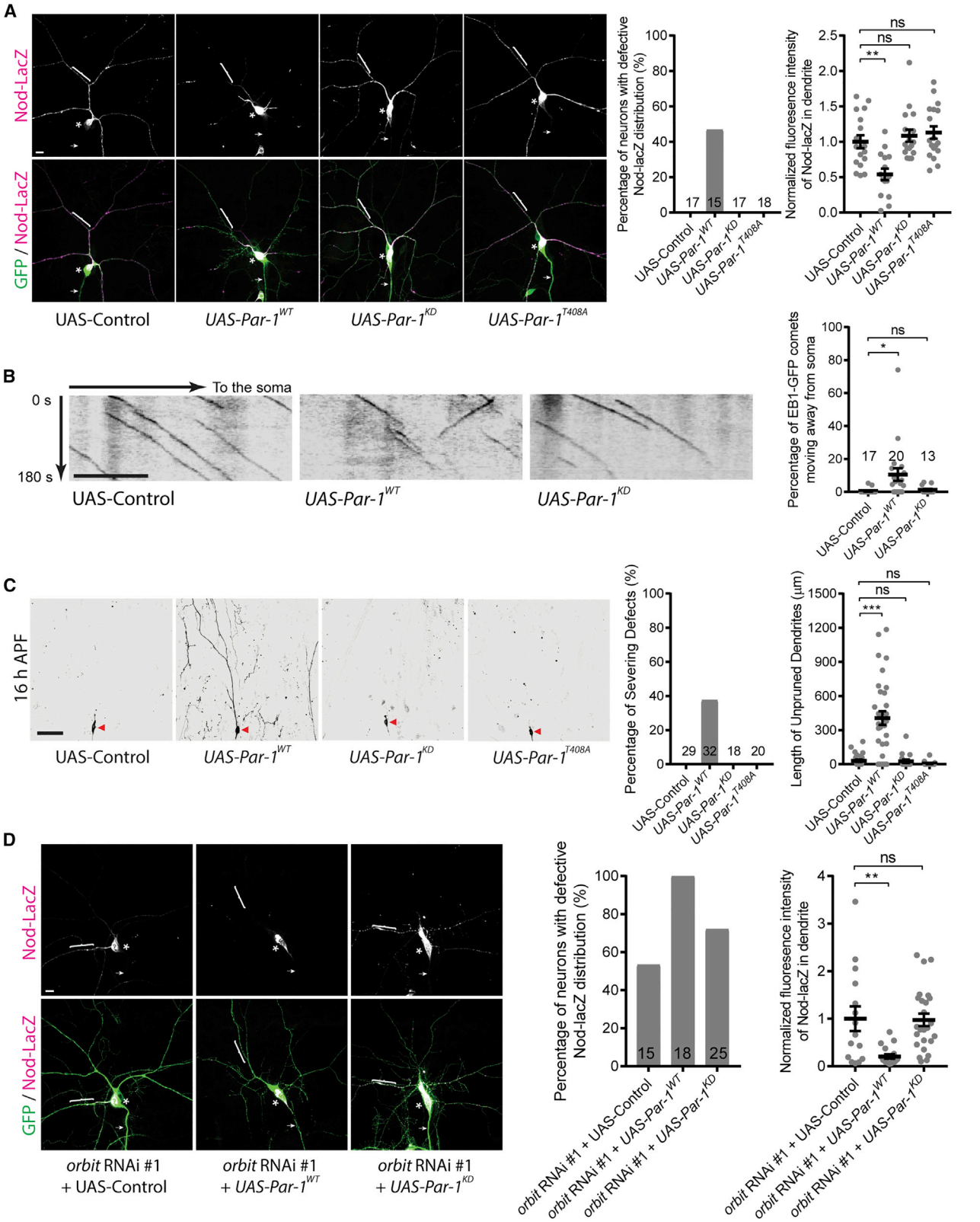

(legend on next page)

To demonstrate that the phenotypes caused by Par-1 overexpression are due to its kinase activity, we overexpressed either a kinase-dead form of Par-1 (Par-1^{KD}) (Nishimura et al., 2004) or a non-phosphorylated form (Par-1^{T408A}) (Lizcano et al., 2004; Timm et al., 2003; Wang et al., 2007), which were shown to be kinase inactive. Overexpression of Par-1^{KD} or Par-1^{T408A} did not affect Nod-LacZ distribution (Figure 4A), EB1-GFP comet directionality (Figure 4B), or dendrite pruning in ddaC neurons (Figure 4C). Moreover, Par-1^{WT} overexpression significantly exacerbated the Nod-lacZ distribution defect in *orbit* RNAi ddaC neurons (Figure 4D), whereas Par-1^{KD} overexpression did not (Figure 4D). Taken together, increased Par-1 function impairs dendritic microtubule orientation and dendrite pruning, phenocopying loss of *orbit* function.

In summary, our data indicate that Orbit regulates dendritic microtubule orientation and dendrite pruning at least partly by antagonizing Par-1 function.

DISCUSSION

In this study, we provide multiple lines of *in vivo* evidence to demonstrate that Orbit is critical for dendrite pruning and the uniform minus-end-out microtubule orientation in the dendrites of ddaC sensory neurons. Orbit is localized on the microtubule lattices in the dendrites of ddaC neurons. It is possible that Orbit functions via the TOG2 domain to associate with and stabilize microtubule lattices in the dendrites, and thereby preserve dendritic minus-end-out microtubule orientation. In agreement with this, mammalian CLASP2, via its TOG2 domain, also associates with microtubule lattices to stabilize microtubules and inhibit microtubule catastrophe (Aher et al., 2018; Leano et al., 2013).

Our previous studies reported that Patronin and Msps maintain the dendritic microtubule orientation in ddaC neurons by counteracting the kinesin-13 microtubule depolymerase Klp10A presumably at the microtubule minus and plus ends, respectively (Tang et al., 2020; Wang et al., 2019). Unexpectedly, Klp10A knockdown, via two previously used RNAi lines, failed to rescue or suppress the *orbit* RNAi phenotypes, suggesting that Orbit and Msps/Patronin use distinct mechanisms or pathways to regulate the dendritic microtubule orientation. Interestingly, in our genetic modifier screen, we identified Par-1 kinase as a suppressor of Orbit. Multiple lines of genetic evidence support the notion that Orbit regulates dendritic microtubule orientation and dendrite pruning at least partly via counteracting Par-1 function. However, we detected no apparent increase in Par-1 protein levels in *orbit* RNAi ddaC neurons (Figure S7C). Moreover, we did not detect a potential interaction between Orbit and Par-1 in S2 cells (Figure S7D). Thus, Orbit indirectly counteracts Par-1 function in ddaC neurons.

The mammalian Par-1 homolog MARK2 can phosphorylate MAPs, such as doublecortin (DCX) or Tau, to release them from microtubule lattices and thereby destabilize microtubules (Biernat et al., 2002; Chen et al., 2006; Drewes et al., 1997; Nishimura et al., 2004; Schaar et al., 2004). In *Drosophila*, Par-1 promotes microtubule breakdown in ddaC neurons largely via inhibition of Tau (Herzmann et al., 2017). We found that Orbit knockdown or Par-1 overexpression reduced Tau levels in the dendrites of ddaC neurons (Figure S8A). Interestingly, further knockdown of Tau exacerbated the dendritic microtubule orientation defect in the *orbit* RNAi background, because the dendritic Nod-lacZ signals were further reduced in *orbit* and *tau* double RNAi neurons (Figure S8B). This finding suggests that Orbit counteracts Par-1 function, which in turn inhibits Tau during the regulation of dendritic microtubule orientation in ddaC sensory neurons.

How does Orbit regulate microtubule minus-end-out orientation in ddaC dendrites? We propose a potential model in which Orbit acts on microtubule lattices to protect microtubules and maintain dendritic microtubule orientation by suppressing Par-1 function (Figure S8C). This model is supported by the following lines of evidence. First, Orbit is localized on the microtubule lattices in the dendrites of ddaC neurons, suggesting that it can protect microtubule fibers from severing or disassembly. Second, the microtubule lattice-binding TOG2 domain is required for Orbit to maintain the minus-end-out microtubule orientation in the dendrites. Third, attenuation of Klp10A, which depolymerizes microtubules from both minus and plus ends (Goodwin and Vale, 2010; Mennella et al., 2005), did not suppress the *orbit* RNAi phenotype, suggesting that Orbit acts independent of Klp10A-mediated depolymerization from the ends. Finally, Par-1 can destabilize microtubules by releasing the microtubule lattice-binding protein Tau. Because in neurons Tau can protect microtubules from severing by the microtubule-severing enzyme katanin (Qiang et al., 2006), we speculate that on Orbit depletion, Par-1 might release Tau and subsequently expose the microtubule lattices to the severing events possibly mediated by microtubule-severing enzymes (e.g., katanin), leading to generation of short microtubule filaments (Figure S8C). Short filaments might be re-oriented randomly and serve as seeds for microtubule polymerization, which leads to mixed microtubule orientation in the dendrites. In agreement with this speculation, overexpression of katanin, which can sever

Figure 4. Par-1 overexpression impairs dendritic microtubule orientation and dendrite pruning

(A) Expression of Nod-lacZ (magenta) in ddaC neurons (green) overexpressing *UAS-Control*, *UAS-Par-1^{WT}*, *UAS-Par-1^{KD}*, and *UAS-Par-1^{T408A}*. The asterisks label the ddaC somas, the arrows point to the axons, and the brackets mark the dendrites (biological replicates = 4). Quantitative analysis of Nod-lacZ distribution in the ddaC dendrites.

(B) Dendritic EB1-GFP kymographs in ddaC neurons overexpressing *UAS-Control*, *UAS-Par-1^{WT}*, and *UAS-Par-1^{KD}*. The horizontal arrow marks the direction toward the soma. The vertical arrow indicates the duration (biological replicates >3). Quantitative analysis of EB1-GFP orientation in the ddaC dendrites.

(C) Dendrites of ddaC neurons overexpressing *UAS-Control*, *UAS-Par-1^{WT}*, *UAS-Par-1^{KD}*, and *UAS-Par-1^{T408A}* at 16 h APF. Red arrowheads point to the soma of ddaC (biological replicates >5). Quantitative analysis of dendrite severing defects and unpruned dendrite length at 16 h APF.

(D) Expression of Nod-lacZ (magenta) in *orbit* RNAi #1 ddaC neurons (green) co-expressing *UAS-Control*, *UAS-Par-1^{WT}*, and *UAS-Par-1^{KD}*. The asterisks label the ddaC somas, the arrows point to the axons, and the brackets mark the dendrites (biological replicates = 4). Quantitative analysis of Nod-lacZ distribution in the ddaC dendrites. The error bars represent SEM. Scale bars represent 10 μm (A, B, and D) and 50 μm (C). *p < 0.05, **p < 0.01, ***p < 0.001. See also Figure S8 and Table S1.

microtubules into short filaments *in vitro* (McNally and Vale, 1993), also impairs dendritic microtubule orientation, as well as dendrite pruning (Tang et al., 2020), phenocopying Orbit depletion. The questions of how microtubules are severed into small microtubule seeds, how microtubules with mixed orientation are generated, and whether impaired microtubule orientation causes dendrite pruning defects can be investigated in future studies.

Limitations of the study

In this study, our genetic data indicate that Orbit regulates microtubule orientation and dendrite pruning partly via suppressing Par-1 function. Although our *in vivo* system provides tremendous opportunities for extensive genetic analysis, the limitations of this system preclude us to pinpoint the cellular mechanism between Orbit and Par-1 in this study. It could be further investigated in future in *in-vitro*-cultured neurons, which are more suitable for super-resolution microscopy and other sophisticated live imaging tools. Moreover, Orbit is not a pruning factor per se but likely regulates dendrite pruning via microtubule orientation.

STAR★METHODS

Detailed methods are provided in the online version of this paper and include the following:

- KEY RESOURCES TABLE
- RESOURCE AVAILABILITY
  - Lead contact
  - Materials availability
  - Data and code availability
- EXPERIMENTAL MODEL AND SUBJECT DETAILS
  - *Drosophila* husbandry and strains
  - S2 cell culture
- METHOD DETAILS
  - Generation of *orbit* transgenes
  - EMS screen, RNAi and MARCM analysis of da neurons
  - Time-lapse imaging of EB1-GFP
  - Microtubule turnover assay
  - RU486/mifepristone treatment
  - Co-immunoprecipitiation
  - Immunofluorescence and antibodies
- QUANTIFICATION AND STATISTICAL ANALYSIS

SUPPLEMENTAL INFORMATION

Supplemental information can be found online at https://doi.org/10.1016/j.celrep.2022.110887.

ACKNOWLEDGMENTS

We thank Y. Jan, D.M. Glover, D. Johnston, B. Lu, A. Prokop, M.M. Rolls, C.E. Sunkel, T. Uemura, D.V. Vactor, H. Wang, the Bloomington Stock Center (BSC), Developmental Studies Hybridoma Bank (DSHB, University of Iowa), Kyoto Stock Center (Japan), and Vienna *Drosophila* RNAi Centre (VDRC; Austria) for generously providing antibodies and fly stocks. We are grateful to M.M. Rolls for providing the technical advice on EB1-GFP imaging. We thank A. Moore and Yu lab members for helpful discussion and technical assistance. F.Y. was supported by Temasek Life Sciences Laboratory Singapore and National Research Foundation Singapore (SBP-P3 and SBP-P8).

AUTHOR CONTRIBUTIONS

S.B., Q.T., Y.W., and F.Y. conceived and designed the study. S.B. performed most of the experiments. Q.T., Y.W., S.S.Y.L., and W.L.Y. conducted some EB1-GFP, Nod-β-gal (β-galactosidase), and MARCM experiments. S.B., Q.T., Y.W., and F.Y. analyzed the data. S.B. and F.Y. wrote the paper.

DECLARATION OF INTERESTS

The authors declare no competing interests.

Received: November 18, 2021
Revised: April 4, 2022
Accepted: May 6, 2022
Published: May 31, 2022

REFERENCES

Aher, A., Kok, M., Sharma, A., Rai, A., Olieric, N., Rodriguez-Garcia, R., Katrukha, E.A., Weinert, T., Olieric, V., Kapitein, L.C., et al. (2018). CLASP suppresses microtubule catastrophes through a single TOG domain. Dev. Cell *46*, 40–58.e48. https://doi.org/10.1016/j.devcel.2018.05.032.

Akhmanova, A., Hoogenraad, C.C., Drabek, K., Stepanova, T., Dortland, B., Verkerk, T., Vermeulen, W., Burgering, B.M., De Zeeuw, C.I., Grosveld, F., and Galjart, N. (2001). Clasps are CLIP-115 and -170 associating proteins involved in the regional regulation of microtubule dynamics in motile fibroblasts. Cell *104*, 923–935. https://doi.org/10.1016/s0092-8674(01)00288-4.

Akhmanova, A., and Steinmetz, M.O. (2008). Tracking the ends: a dynamic protein network controls the fate of microtubule tips. Nat. Rev. Mol. Cell Biol. *9*, 309–322. https://doi.org/10.1038/nrm2369.

Akhmanova, A., and Steinmetz, M.O. (2015). Control of microtubule organization and dynamics: two ends in the limelight. Nat. Rev. Mol. Cell Biol. *16*, 711–726. https://doi.org/10.1038/nrm4084.

Al-Bassam, J., and Chang, F. (2011). Regulation of microtubule dynamics by TOG-domain proteins XMAP215/Dis1 and CLASP. Trends Cell Biol. *21*, 604–614. https://doi.org/10.1016/j.tcb.2011.06.007.

Baas, P.W., and Lin, S. (2011). Hooks and comets: the story of microtubule polarity orientation in the neuron. Dev. Neurobiol. *71*, 403–418. https://doi.org/10.1002/dneu.20818.

Barlan, K., Lu, W., and Gelfand, V.I. (2013). The microtubule-binding protein ensconsin is an essential cofactor of kinesin-1. Curr. Biol. *23*, 317–322. https://doi.org/10.1016/j.cub.2013.01.008.

Beffert, U., Dillon, G.M., Sullivan, J.M., Stuart, C.E., Gilbert, J.P., Kambouris, J.A., and Ho, A. (2012). Microtubule plus-end tracking protein CLASP2 regulates neuronal polarity and synaptic function. J. Neurosci. *32*, 13906–13916. https://doi.org/10.1523/JNEUROSCI.2108-12.2012.

Biernat, J., Wu, Y.Z., Timm, T., Zheng-Fischhofer, Q., Mandelkow, E., Meijer, L., and Mandelkow, E.M. (2002). Protein kinase MARK/PAR-1 is required for neurite outgrowth and establishment of neuronal polarity. Mol. Biol. Cell *13*, 4013–4028. https://doi.org/10.1091/mbc.02-03-0046.

Bu, S., Yong, W.L., Lim, B.J.W., Kondo, S., and Yu, F. (2021). A systematic analysis of microtubule-destabilizing factors during dendrite pruning in Drosophila. EMBO Rep. *22*, e52679. https://doi.org/10.15252/embr.202152679.

Chen, Y.M., Wang, Q.J., Hu, H.S., Yu, P.C., Zhu, J., Drewes, G., Piwnica-Worms, H., and Luo, Z.G. (2006). Microtubule affinity-regulating kinase 2 functions downstream of the PAR-3/PAR-6/atypical PKC complex in regulating hippocampal neuronal polarity. Proc. Natl. Acad. Sci. U S A *103*, 8534–8539. https://doi.org/10.1073/pnas.0509955103.

Clark, I.E., Jan, L.Y., and Jan, Y.N. (1997). Reciprocal localization of Nod and kinesin fusion proteins indicates microtubule polarity in the Drosophila oocyte, epithelium, neuron and muscle. Development *124*, 461–470.

Dix, C.I., Soundararajan, H.C., Dzhindzhev, N.S., Begum, F., Suter, B., Ohkura, H., Stephens, E., and Bullock, S.L. (2013). Lissencephaly-1 promotes the

recruitment of dynein and dynactin to transported mRNAs. J. Cell Biol. *202*, 479–494. https://doi.org/10.1083/jcb.201211052.

Doerflinger, H., Benton, R., Shulman, J.M., and St Johnston, D. (2003). The role of PAR-1 in regulating the polarised microtubule cytoskeleton in the Drosophila follicular epithelium. Development *130*, 3965–3975. https://doi.org/10.1242/dev.00616.

Drewes, G., Ebneth, A., Preuss, U., Mandelkow, E.M., and Mandelkow, E. (1997). MARK, a novel family of protein kinases that phosphorylate microtubule-associated proteins and trigger microtubule disruption. Cell *89*, 297–308. https://doi.org/10.1016/s0092-8674(00)80208-1.

Efimov, A., Kharitonov, A., Efimova, N., Loncarek, J., Miller, P.M., Andreyeva, N., Gleeson, P., Galjart, N., Maia, A.R., McLeod, I.X., et al. (2007). Asymmetric CLASP-dependent nucleation of noncentrosomal microtubules at the trans-Golgi network. Dev. Cell *12*, 917–930. https://doi.org/10.1016/j.devcel.2007.04.002.

Feng, C., Thyagarajan, P., Shorey, M., Seebold, D.Y., Weiner, A.T., Albertson, R.M., Rao, K.S., Sagasti, A., Goetschius, D.J., and Rolls, M.M. (2019). Patronin-mediated minus end growth is required for dendritic microtubule polarity. J. Cell Biol. *218*, 2309–2328. https://doi.org/10.1083/jcb.201810155.

Goodwin, P.R., Sasaki, J.M., and Juo, P. (2012). Cyclin-dependent kinase 5 regulates the polarized trafficking of neuropeptide-containing dense-core vesicles in Caenorhabditis elegans motor neurons. J. Neurosci. *32*, 8158–8172. https://doi.org/10.1523/JNEUROSCI.0251-12.2012.

Goodwin, S.S., and Vale, R.D. (2010). Patronin regulates the microtubule network by protecting microtubule minus ends. Cell *143*, 263–274. https://doi.org/10.1016/j.cell.2010.09.022.

Grueber, W.B., Ye, B., Moore, A.W., Jan, L.Y., and Jan, Y.N. (2003). Dendrites of distinct classes of Drosophila sensory neurons show different capacities for homotypic repulsion. Curr. Biol. *13*, 618–626. https://doi.org/10.1016/s0960-9822(03)00207-0.

Guo, S., and Kemphues, K.J. (1995). par-1, a gene required for establishing polarity in C. elegans embryos, encodes a putative Ser/Thr kinase that is asymmetrically distributed. Cell *81*, 611–620. https://doi.org/10.1016/0092-8674(95)90082-9.

Han, C., Song, Y., Xiao, H., Wang, D., Franc, N.C., Jan, L.Y., and Jan, Y.N. (2014). Epidermal cells are the primary phagocytes in the fragmentation and clearance of degenerating dendrites in Drosophila. Neuron *81*, 544–560. https://doi.org/10.1016/j.neuron.2013.11.021.

Herzmann, S., Gotzelmann, I., Reekers, L.F., and Rumpf, S. (2018). Spatial regulation of microtubule disruption during dendrite pruning in Drosophila. Development *145*. https://doi.org/10.1242/dev.156950.

Herzmann, S., Krumkamp, R., Rode, S., Kintrup, C., and Rumpf, S. (2017). PAR-1 promotes microtubule breakdown during dendrite pruning in Drosophila. EMBO J. *36*, 1981–1991. https://doi.org/10.15252/embj.201695890.

Honnappa, S., Gouveia, S.M., Weisbrich, A., Damberger, F.F., Bhavesh, N.S., Jawhari, H., Grigoriev, I., van Rijssel, F.J., Buey, R.M., Lawera, A., et al. (2009). An EB1-binding motif acts as a microtubule tip localization signal. Cell *138*, 366–376. https://doi.org/10.1016/j.cell.2009.04.065.

Hur, E.M., Saijilafu, Lee, B.D., Kim, S.J., Xu, W.L., and Zhou, F.Q. (2011). GSK3 controls axon growth via CLASP-mediated regulation of growth cone microtubules. Genes Dev. *25*, 1968–1981. https://doi.org/10.1101/gad.17015911.

Inoue, Y.H., do Carmo Avides, M., Shiraki, M., Deak, P., Yamaguchi, M., Nishimoto, Y., Matsukage, A., and Glover, D.M. (2000). Orbit, a novel microtubule-associated protein essential for mitosis in Drosophila melanogaster. J. Cell Biol. *149*, 153–166. https://doi.org/10.1083/jcb.149.1.153.

Kirilly, D., Gu, Y., Huang, Y., Wu, Z., Bashirullah, A., Low, B.C., Kolodkin, A.L., Wang, H., and Yu, F. (2009). A genetic pathway composed of Sox14 and Mical governs severing of dendrites during pruning. Nat. Neurosci. *12*, 1497–1505. https://doi.org/10.1038/nn.2415.

Kuo, C.T., Jan, L.Y., and Jan, Y.N. (2005). Dendrite-specific remodeling of Drosophila sensory neurons requires matrix metalloproteases, ubiquitin-proteasome, and ecdysone signaling. Proc. Natl. Acad. Sci. U S A *102*, 15230–15235. https://doi.org/10.1073/pnas.0507393102.

Lawrence, E.J., Zanic, M., and Rice, L.M. (2020). CLASPs at a glance. J. Cell Sci. *133*, jcs243097. https://doi.org/10.1242/jcs.243097.

Leano, J.B., Rogers, S.L., and Slep, K.C. (2013). A cryptic TOG domain with a distinct architecture underlies CLASP-dependent bipolar spindle formation. Structure *21*, 939–950. https://doi.org/10.1016/j.str.2013.04.018.

Lee, H., Engel, U., Rusch, J., Scherrer, S., Sheard, K., and Van Vactor, D. (2004). The microtubule plus end tracking protein Orbit/MAST/CLASP acts downstream of the tyrosine kinase Abl in mediating axon guidance. Neuron *42*, 913–926. https://doi.org/10.1016/j.neuron.2004.05.020.

Lee, H.H., Jan, L.Y., and Jan, Y.N. (2009). Drosophila IKK-related kinase Ik2 and Katanin p60-like 1 regulate dendrite pruning of sensory neuron during metamorphosis. Proc. Natl. Acad. Sci. U S A *106*, 6363–6368. https://doi.org/10.1073/pnas.0902051106.

Lemos, C.L., Sampaio, P., Maiato, H., Costa, M., Omel'yanchuk, L.V., Liberal, V., and Sunkel, C.E. (2000). Mast, a conserved microtubule-associated protein required for bipolar mitotic spindle organization. EMBO J. *19*, 3668–3682. https://doi.org/10.1093/emboj/19.14.3668.

Lizcano, J.M., Goransson, O., Toth, R., Deak, M., Morrice, N.A., Boudeau, J., Hawley, S.A., Udd, L., Makela, T.P., Hardie, D.G., and Alessi, D.R. (2004). LKB1 is a master kinase that activates 13 kinases of the AMPK subfamily, including MARK/PAR-1. EMBO J. *23*, 833–843. https://doi.org/10.1038/sj.emboj.7600110.

Lu, W., Fox, P., Lakonishok, M., Davidson, M.W., and Gelfand, V.I. (2013). Initial neurite outgrowth in Drosophila neurons is driven by kinesin-powered microtubule sliding. Curr. Biol. *23*, 1018–1023. https://doi.org/10.1016/j.cub.2013.04.050.

Lu, W., Lakonishok, M., and Gelfand, V.I. (2015). Kinesin-1-powered microtubule sliding initiates axonal regeneration in Drosophila cultured neurons. Mol. Biol. Cell *26*, 1296–1307. https://doi.org/10.1091/mbc.E14-10-1423.

Luo, L., and O'Leary, D.D. (2005). Axon retraction and degeneration in development and disease. Annu. Rev. Neurosci. *28*, 127–156. https://doi.org/10.1146/annurev.neuro.28.061604.135632.

Maiato, H., Sampaio, P., Lemos, C.L., Findlay, J., Carmena, M., Earnshaw, W.C., and Sunkel, C.E. (2002). MAST/Orbit has a role in microtubule-kinetochore attachment and is essential for chromosome alignment and maintenance of spindle bipolarity. J. Cell Biol. *157*, 749–760. https://doi.org/10.1083/jcb.200201101.

Mathe, E., Inoue, Y.H., Palframan, W., Brown, G., and Glover, D.M. (2003). Orbit/Mast, the CLASP orthologue of Drosophila, is required for asymmetric stem cell and cystocyte divisions and development of the polarised microtubule network that interconnects oocyte and nurse cells during oogenesis. Development *130*, 901–915. https://doi.org/10.1242/dev.00315.

Matsubara, D., Horiuchi, S.Y., Shimono, K., Usui, T., and Uemura, T. (2011). The seven-pass transmembrane cadherin Flamingo controls dendritic self-avoidance via its binding to a LIM domain protein, Espinas, in Drosophila sensory neurons. Genes Dev. *25*, 1982–1996. https://doi.org/10.1101/gad.16531611.

Mattie, F.J., Stackpole, M.M., Stone, M.C., Clippard, J.R., Rudnick, D.A., Qiu, Y., Tao, J., Allender, D.L., Parmar, M., and Rolls, M.M. (2010). Directed microtubule growth, +TIPs, and kinesin-2 are required for uniform microtubule polarity in dendrites. Curr. Biol. *20*, 2169–2177. https://doi.org/10.1016/j.cub.2010.11.050.

McNally, F.J., and Vale, R.D. (1993). Identification of katanin, an ATPase that severs and disassembles stable microtubules. Cell *75*, 419–429. https://doi.org/10.1016/0092-8674(93)90377-3.

Mennella, V., Rogers, G.C., Rogers, S.L., Buster, D.W., Vale, R.D., and Sharp, D.J. (2005). Functionally distinct kinesin-13 family members cooperate to regulate microtubule dynamics during interphase. Nat. Cell Biol. *7*, 235–245. https://doi.org/10.1038/ncb1222.

Nishimura, I., Yang, Y., and Lu, B. (2004). PAR-1 kinase plays an initiator role in a temporally ordered phosphorylation process that confers tau toxicity in

Drosophila. Cell *116*, 671–682. https://doi.org/10.1016/s0092-8674(04)00170-9.

Ori-McKenney, K.M., Jan, L.Y., and Jan, Y.N. (2012). Golgi outposts shape dendrite morphology by functioning as sites of acentrosomal microtubule nucleation in neurons. Neuron *76*, 921–930. https://doi.org/10.1016/j.neuron.2012.10.008.

Qiang, L., Yu, W., Andreadis, A., Luo, M., and Baas, P.W. (2006). Tau protects microtubules in the axon from severing by katanin. J. Neurosci. *26*, 3120–3129. https://doi.org/10.1523/JNEUROSCI.5392-05.2006.

Riccomagno, M.M., and Kolodkin, A.L. (2015). Sculpting neural circuits by axon and dendrite pruning. Annu. Rev. Cell Dev. Biol. *31*, 779–805. https://doi.org/10.1146/annurev-cellbio-100913-013038.

Rolls, M.M., Satoh, D., Clyne, P.J., Henner, A.L., Uemura, T., and Doe, C.Q. (2007). Polarity and intracellular compartmentalization of Drosophila neurons. Neural Dev. *2*, 7. https://doi.org/10.1186/1749-8104-2-7.

Roos, J., Hummel, T., Ng, N., Klambt, C., and Davis, G.W. (2000). Drosophila Futsch regulates synaptic microtubule organization and is necessary for synaptic growth. Neuron *26*, 371–382. https://doi.org/10.1016/s0896-6273(00)81170-8.

Rui, M., Ng, K.S., Tang, Q., Bu, S., and Yu, F. (2020). Protein phosphatase PP2A regulates microtubule orientation and dendrite pruning in Drosophila. EMBO Rep. *21*, e48843. https://doi.org/10.15252/embr.201948843.

Schaar, B.T., Kinoshita, K., and McConnell, S.K. (2004). Doublecortin microtubule affinity is regulated by a balance of kinase and phosphatase activity at the leading edge of migrating neurons. Neuron *41*, 203–213. https://doi.org/10.1016/s0896-6273(03)00843-2.

Schuldiner, O., and Yaron, A. (2015). Mechanisms of developmental neurite pruning. Cell. Mol. Life Sci. *72*, 101–119. https://doi.org/10.1007/s00018-014-1729-6.

Shimono, K., Fujimoto, A., Tsuyama, T., Yamamoto-Kochi, M., Sato, M., Hattori, Y., Sugimura, K., Usui, T., Kimura, K., and Uemura, T. (2009). Multidendritic sensory neurons in the adult Drosophila abdomen: origins, dendritic morphology, and segment- and age-dependent programmed cell death. Neural Dev. *4*, 37. https://doi.org/10.1186/1749-8104-4-37.

Stepanova, T., Slemmer, J., Hoogenraad, C.C., Lansbergen, G., Dortland, B., De Zeeuw, C.I., Grosveld, F., van Cappellen, G., Akhmanova, A., and Galjart, N. (2003). Visualization of microtubule growth in cultured neurons via the use of EB3-GFP (end-binding protein 3-green fluorescent protein). J. Neurosci. *23*, 2655–2664.

Stone, M.C., Roegiers, F., and Rolls, M.M. (2008). Microtubules have opposite orientation in axons and dendrites of Drosophila neurons. Mol. Biol. Cell *19*, 4122–4129. https://doi.org/10.1091/mbc.E07-10-1079.

Sun, L., Cui, L., Liu, Z., Wang, Q., Xue, Z., Wu, M., Sun, T., Mao, D., Ni, J., Pastor-Pareja, J.C., and Liang, X. (2021). Katanin p60-like 1 sculpts the cytoskeleton in mechanosensory cilia. J. Cell Biol. *220*, e202004184. https://doi.org/10.1083/jcb.202004184.

Tang, Q., Rui, M., Bu, S., Wang, Y., Chew, L.Y., and Yu, F. (2020). A microtubule polymerase is required for microtubule orientation and dendrite pruning in Drosophila. EMBO J. *39*, e103549. https://doi.org/10.15252/embj.2019103549.

Tao, J., Feng, C., and Rolls, M.M. (2016). The microtubule-severing protein fidgetin acts after dendrite injury to promote their degeneration. J. Cell Sci. *129*, 3274–3281. https://doi.org/10.1242/jcs.188540.

Terman, J.R., Mao, T., Pasterkamp, R.J., Yu, H.H., and Kolodkin, A.L. (2002). MICALs, a family of conserved flavoprotein oxidoreductases, function in plexin-mediated axonal repulsion. Cell *109*, 887–900. https://doi.org/10.1016/s0092-8674(02)00794-8.

Tian, X., Zhu, M., Li, L., and Wu, C. (2013). Identifying protein-protein interaction in Drosophila adult heads by Tandem Affinity Purification (TAP). J. Vis. Exp., 50968. https://doi.org/10.3791/50968.

Timm, T., Li, X.Y., Biernat, J., Jiao, J., Mandelkow, E., Vandekerckhove, J., and Mandelkow, E.M. (2003). MARKK, a Ste20-like kinase, activates the polarity-inducing kinase MARK/PAR-1. EMBO J. *22*, 5090–5101. https://doi.org/10.1093/emboj/cdg447.

Truman, J.W. (1990). Metamorphosis of the central nervous system of Drosophila. J. Neurobiol. *21*, 1072–1084. https://doi.org/10.1002/neu.480210711.

Venken, K.J., Carlson, J.W., Schulze, K.L., Pan, H., He, Y., Spokony, R., Wan, K.H., Koriabine, M., de Jong, P.J., White, K.P., et al. (2009). Versatile P[acman] BAC libraries for transgenesis studies in Drosophila melanogaster. Nat. Methods *6*, 431–434. https://doi.org/10.1038/nmeth.1331.

Wang, J.W., Imai, Y., and Lu, B. (2007). Activation of PAR-1 kinase and stimulation of tau phosphorylation by diverse signals require the tumor suppressor protein LKB1. J. Neurosci. *27*, 574–581. https://doi.org/10.1523/JNEUROSCI.5094-06.2007.

Wang, Y., Rui, M., Tang, Q., Bu, S., and Yu, F. (2019). Patronin governs minus-end-out orientation of dendritic microtubules to promote dendrite pruning in Drosophila. Elife *8*, e39964. https://doi.org/10.7554/eLife.3996.

Williams, D.W., and Truman, J.W. (2005). Cellular mechanisms of dendrite pruning in Drosophila: insights from in vivo time-lapse of remodeling dendritic arborizing sensory neurons. Development *132*, 3631–3642. https://doi.org/10.1242/dev.01928.

Witte, H., Neukirchen, D., and Bradke, F. (2008). Microtubule stabilization specifies initial neuronal polarization. J. Cell Biol. *180*, 619–632. https://doi.org/10.1083/jcb.200707042.

Yan, J., Chao, D.L., Toba, S., Koyasako, K., Yasunaga, T., Hirotsune, S., and Shen, K. (2013). Kinesin-1 regulates dendrite microtubule polarity in Caenorhabditis elegans. Elife *2*, e00133. https://doi.org/10.7554/eLife.00133.

Yu, F., and Schuldiner, O. (2014). Axon and dendrite pruning in Drosophila. Curr. Opin. Neurobiol. *27*, 192–198. https://doi.org/10.1016/j.conb.2014.04.005.

Zheng, Y., Wildonger, J., Ye, B., Zhang, Y., Kita, A., Younger, S.H., Zimmerman, S., Jan, L.Y., and Jan, Y.N. (2008). Dynein is required for polarized dendritic transport and uniform microtubule orientation in axons. Nat. Cell Biol. *10*, 1172–1180. https://doi.org/10.1038/ncb1777.

STAR★METHODS

KEY RESOURCES TABLE

REAGENT or RESOURCE	SOURCE	IDENTIFIER
Antibodies		
Mouse monoclonal anti-Futsch	Developmental Studies Hybridoma Bank	Cat# 22C10, RRID: AB_528403
Mouse monoclonal anti-β-Galactosidase	Promega	Cat# 378A; RRID: AB_2313752
Rabbit polyclonal anti-GFP	Invitrogen	Cat# A-11122; RRID: AB_ 221569
Rabbit polyclonal anti-Tau	(Doerflinger et al., 2003)	N/A
Rabbit polyclonal anti-Orbit	(Lemos et al., 2000)	N/A
Mouse monoclonal anti-α-Tubulin	Sigma	Cat# T9026, RRID: AB_477593
Anti-c-Myc–Peroxidase antibody	Sigma-Aldrich	Cat# A5598; RRID: AB_439682
Anti-HA-Peroxidase antibody	Roche	Cat# 12013819001; RRID: AB_390917
Monoclonal Anti-Flag M2-Peroxidase antibody	Sigma-Aldrich	Cat# A8592; RRID: AB_439702
Alexa Fluor® 488 AffiniPure Goat Anti-Rabbit IgG (H+L)	Jackson ImmunoResearch Laboratories	Cat# 111-545-003; RRID: AB_2338046
Cy™3 AffiniPure goat polyclonal anti-mouse IgG (H+L)	Jackson ImmunoResearch Laboratories	Cat# 115-165-003; RRID: AB_2338680
Cy™3 AffiniPure goat polyclonal anti-rabbit IgG (H+L)	Jackson ImmunoResearch Laboratories	Cat# 111-165-003; RRID: AB_2338000
Alexa Fluor® 647 AffiniPure Goat Anti-Horseradish Peroxidase	Jackson ImmunoResearch Laboratories	Cat# 123-605-021; RRID: AB_2338967
Chemicals, peptides, and recombinant proteins		
Mifepristone	Sigma-Aldrich	Cat# M8046
Halocarbon oil 27	Santa Cruz	Cat# sc-250077
Express Five™ SFM	Gibco	Cat# 10486025
IP Lysis buffer	Pierce	Cat# 87788
Protein A/G Agarose	Pierce	Cat# 20421
Glutaraldehyde	Sigma-Aldrich	Cat# G6257
Formaldehyde	Polysciences Inc.	Cat# NC9200219
Glycerol	Invitrogen	Cat# 15514011
Vectashield	Vector Laboratories	Cat# H-1000
Critical commercial assays		
Axygen Plasmid Miniprep Kit	Axygen	Cat# AP-MN-P-250
pENTR™/D-TOPO™ Cloning Kit	Invitrogen	Cat# K240020
QuikChange Lightning Site-directed Mutagenesis Kit	Agilent Technologies	Cat# 210518
Gateway™ LR Clonase™ II Enzyme mix	Invitrogen	Cat# 11791020
BACMAX™ DNA Purification Kit	Analisa Scientific	Cat# BMAX044
Effectene Transfection Reagent	Qiagen	Cat# 301425
Experimental models: Organisms/strains		
Drosophila melanogaster: *UAS-Mical$^{N\text{-}ter}$*	(Terman et al., 2002)	N/A
Drosophila melanogaster: *ppk-Gal4* (Chr. II and III)	(Grueber et al., 2003)	N/A
Drosophila melanogaster: *SOP-flp* (Chr. II and III)	(Matsubara et al., 2011)	N/A
Drosophila melanogaster: *UAS-EB1-GFP*	(Stone et al., 2008)	N/A
Drosophila melanogaster: *UAS-Kin-β-Gal*	(Clark et al., 1997)	N/A
Drosophila melanogaster: *orbit^{3}*	(Inoue et al., 2000)	N/A
Drosophila melanogaster: *orbit^{4}*	(Inoue et al., 2000)	N/A

(*Continued on next page*)

Continued

REAGENT or RESOURCE	SOURCE	IDENTIFIER
Drosophila melanogaster: *g-orbit*	(Inoue et al., 2000)	N/A
Drosophila melanogaster: *UAS-Orbit-GFP*	(Lee et al., 2004)	N/A
Drosophila melanogaster: *CLIP-190^{KO}*	(Dix et al., 2013)	N/A
Drosophila melanogaster: *UAS-Par-1^{WT}*	(Wang et al., 2007)	N/A
Drosophila melanogaster: *UAS-Par-1^{KD}*	(Wang et al., 2007)	N/A
Drosophila melanogaster: *UAS-Par-1^{T408A}*	(Wang et al., 2007)	N/A
Drosophila melanogaster: *orbit^{464}*	This study	N/A
Drosophila melanogaster: *g-orbit-tdGFP*	This study	N/A
Drosophila melanogaster: *UASp-Orbit^{FL}*	This study	N/A
Drosophila melanogaster: *UASp-GFP-Orbit*	This study	N/A
Drosophila melanogaster: *UASp-Orbit$^{\Delta TOG1}$*	This study	N/A
Drosophila melanogaster: *UASp-Orbit$^{\Delta TOG2}$*	This study	N/A
Drosophila melanogaster: *UASp-Orbit$^{\Delta TOG3}$*	This study	N/A
Drosophila melanogaster: *UASp-Orbit$^{\Delta SxIP}$*	This study	N/A
Drosophila melanogaster: *UASp-Orbit$^{\Delta CLIP\text{-}ID}$*	This study	N/A
Drosophila melanogaster: *UASp-Orbit$^{TOG1,2\text{-}linker}$*	This study	N/A
Drosophila melanogaster: *UASp-Orbit^{TOG2}*	This study	N/A
Drosophila melanogaster: *UAS-Orbit*	This study	N/A
Drosophila melanogaster: *UAS-Orbit-HA*	This study	N/A
Drosophila melanogaster: *UAS-Orbit-CTAP*	This study	N/A
Drosophila melanogaster: *UAS-mCD8::GFP* (Chr. II and III)	Bloomington Stock Centre (BDSC)	RRID: BDSC_5130; RRID: BDSC_5137
Drosophila melanogaster: *FRT2A*	BDSC	RRID: BDSC_1997
Drosophila melanogaster: *UAS-Dicer2* (Chr. II and III)	BDSC	RRID: BDSC_24650; RRID: BDSC_24651
Drosophila melanogaster: *FRT2A, tubP-Gal80*	BDSC	RRID: BDSC_5190
Drosophila melanogaster: *Gal4$^{109(2)80}$, UAS-mCD8::GFP*	BDSC	RRID: BDSC_8768
Drosophila melanogaster: *Gal4$^{4\text{-}77}$*	BDSC	RRID: BDSC_8737
Drosophila melanogaster: *UAS-Nod-β-Gal*	BDSC	RRID: BDSC_9912
Drosophila melanogaster: *ppk-CD4-tdGFP*	BDSC	RRID: BDSC_35843
Drosophila melanogaster: *GSG2295-Gal4*	BDSC	RRID: BDSC_40266
Drosophila melanogaster: *UASp-αTub84B-tdEOS* (Chr. II and III)	BDSC	RRID: BDSC_51313; RRID: BDSC_51314
Drosophila melanogaster: *orbit RNAi #1*	BDSC	RRID: BDSC_35442
Drosophila melanogaster: *mCherry RNAi* (control RNAi)	BDSC	RRID: BDSC_35785
Drosophila melanogaster: *CLIP-190 RNAi #1*	BDSC	RRID: BDSC_31265
Drosophila melanogaster: *par-1 RNAi #1*	BDSC	RRID: BDSC_32410
Drosophila melanogaster: *par-1 RNAi #2*	BDSC	RRID: BDSC_35342
Drosophila melanogaster: *par-1-KI-GFP*	BDSC	RRID: BDSC_64452
Drosophila melanogaster: *klp10A RNAi*	BDSC	RRID: BDSC_33963
Drosophila melanogaster: *spas RNAi*	BDSC	RRID: BDSC_53331
Drosophila melanogaster: *spas RNAi*	BDSC	RRID: BDSC_27570
Drosophila melanogaster: *fign RNAi*	BDSC	RRID: BDSC_38266
Drosophila melanogaster: *kat-60L1 RNAi*	BDSC	RRID: BDSC_36866
Drosophila melanogaster: *stai RNAi*	BDSC	RRID: BDSC_36902
Drosophila melanogaster: *sgg RNAi*	BDSC	RRID: BDSC_35364
Drosophila melanogaster: *sgg RNAi*	BDSC	RRID: BDSC_38293
Drosophila melanogaster: *ptrn RNAi*	BDSC	RRID: BDSC_36659
Drosophila melanogaster: *tacc RNAi*	BDSC	RRID: BDSC_65982
Drosophila melanogaster: *khc RNAi*	BDSC	RRID: BDSC_35770

(*Continued on next page*)

Continued

REAGENT or RESOURCE	SOURCE	IDENTIFIER
Drosophila melanogaster: *dhc64C RNAi*	BDSC	RRID: BDSC_36698
Drosophila melanogaster: *shot RNAi*	BDSC	RRID: BDSC_64041
Drosophila melanogaster: *γtub23C RNAi*	BDSC	RRID: BDSC_31204
Drosophila melanogaster: orbit RNAi #2	Vienna *Drosophila* RNAi Centre (VDRC)	KK-108620
Drosophila melanogaster: γtub37C RNAi (control RNAi)	VDRC	GD-25271
Drosophila melanogaster: GCC185 RNAi #1	VDRC	GD-26221
Drosophila melanogaster: GCC185 RNAi #2	VDRC	KK-106596
Drosophila melanogaster: CLIP-190 RNAi #2	VDRC	KK-107824
Drosophila melanogaster: tau RNAi #1	VDRC	GD-25023
Drosophila melanogaster: tau RNAi #2	VDRC	GD-25024
Drosophila melanogaster: klp10A RNAi	VDRC	GD-41534
Drosophila melanogaster: spas RNAi	VDRC	GD-33110
Drosophila melanogaster: kat-60 RNAi	VDRC	GD-38369
Drosophila melanogaster: kat-60 RNAi	VDRC	KK-106487
Drosophila melanogaster: fign RNAi	VDRC	GD-24746
Drosophila melanogaster: kat-60L1 RNAi	VDRC	GD-31598
Drosophila melanogaster: kat-60L1 RNAi	VDRC	GD-31599
Drosophila melanogaster: kat-60L1 RNAi	VDRC	KK-108168
Drosophila melanogaster: efa6 RNAi	VDRC	SH-330083
Drosophila melanogaster: msps RNAi	VDRC	GD-21982
Drosophila melanogaster: unc-104 RNAi	VDRC	GD-47171
Drosophila melanogaster: kap3 RNAi	VDRC	KK-103548
Drosophila melanogaster: khc RNAi	VDRC	GD-44338
Drosophila melanogaster: ncd RNAi	VDRC	GD-22571
Drosophila melanogaster: futsch RNAi	VDRC	GD-6972
Drosophila melanogaster: eb1 RNAi	VDRC	GD-24451
Oligonucleotides		
pTW	DGRC	Cat# 1129
pTWH	DGRC	Cat# 1100
pUAST-CTAP	(Tian et al., 2013)	N/A
pPW	DGRC	Cat# 1130
pPGW	DGRC	Cat# 1071
pAHW	DGRC	Cat# 1095
pAMW	DGRC	Cat# 1103
pAFW	DGRC	Cat# 1111
pAWF	DGRC	Cat# 1112
EST LD31673	DGRC	Cat# 6665
EST FI04457	DGRC	Cat# 1621676
EST SD05712	DGRC	Cat# 5335
BAC clone CH322-62N12	BACPAC Resource Center	N/A
Recombinant DNA		
Plasmid: pENTR-Orbit	This paper	N/A
Plasmid: pTW-Orbit	This paper	N/A
Plasmid: pTWH-Orbit	This paper	N/A
Plasmid: pUAST-Orbit-CTAP	This paper	N/A
Plasmid: pPW-Orbit^{FL}	This paper	N/A
Plasmid: pPGW-Orbit^{FL}	This paper	N/A

(*Continued on next page*)

Continued		
REAGENT or RESOURCE	SOURCE	IDENTIFIER
Plasmid: pPW-Orbit$^{\Delta TOG1}$	This paper	N/A
Plasmid: pPW-Orbit$^{\Delta TOG2}$	This paper	N/A
Plasmid: pPW-Orbit$^{\Delta TOG3}$	This paper	N/A
Plasmid: pPW-Orbit$^{\Delta SxIP}$	This paper	N/A
Plasmid: pPW-Orbit$^{\Delta CLIP\text{-}ID}$	This paper	N/A
Plasmid: pPW-Orbit$^{TOG1,2\text{-}linker}$	This paper	N/A
Plasmid: pPW-Orbit^{TOG2}	This paper	N/A
Plasmid: pENTR-tdGFP	This paper	N/A
Plasmid: pAHW-Orbit	This paper	N/A
Plasmid: pAMW-Orbit	This paper	N/A
Plasmid: pAFW-GCC185	This paper	N/A
Plasmid: pAWF-Par-1	This paper	N/A
BAC clone: CH322-62N12-Orbit-tdGFP	This paper	N/A
Software and algorithms		
Adobe Photoshop	Adobe	https://www.adobe.com/products/photoshop.html
Adobe Illustrator	Adobe	https://www.adobe.com/products/illustrator.html
Fiji (ImageJ)	NIH	https://imagej.net/Fiji/Downloads
GraphPad Prism 8	GraphPad	https://www.graphpad.com/scientific-software/prism/
Excel	Microsoft	https://www.microsoft.com/en-us/microsoft-365/excel
Olympus FV3000 confocal microscopy	Olympus	https://www.olympus-lifescience.com/en/laser-scanning/fv3000/
Leica TCS SP2 confocal microscopy	Leica	https://www.leica-microsystems.com/products/confocal-microscopes/p/leica-tcs-sp2/
Biorender	Biorender	https://biorender.com/

RESOURCE AVAILABILITY

Lead contact

Further information and requests for resource and reagents should be directed to and will be fulfilled by the lead contact Fengwei Yu (fengwei@tll.org.sg).

Materials availability

Most materials are commercially available. All unique reagents generated in this study are available from the Lead contact without restriction.

Data and code availability

- All data reported in this paper will be shared by the lead contact upon request.
- This paper does not report original code.
- Any additional information required to reanalyze the data reported in this paper is available from the lead contact upon request.

EXPERIMENTAL MODEL AND SUBJECT DETAILS

Drosophila husbandry and strains

All *Drosophila* stocks and crosses were maintained in standard cornmeal media at 25°C. All fly genotypes used in this study are listed in the key resources table and Table S1. The third instar larvae or early pupae at 0, 16 or 19 h APF (both male and female) were used in this study. *ppk-Gal4* on Chromosome II and III (Grueber et al., 2003), *SOP-flp* (#42) (Matsubara et al., 2011), *UAS-Mical^{Nterm}* (Terman et al., 2002), *UAS-EB1-GFP* (Stone et al., 2008), *UAS-Kin-β-Gal* (Clark et al., 1997), *orbit^{3}*, *orbit^{4}*, *g-orbit* (Inoue et al., 2000), *UAS-Orbit-GFP* (Lee et al., 2004), *CLIP-190^{KO}* (Dix et al., 2013), *UAS-Par-1^{WT}*, *UAS-Par-1^{KD}*, *UAS-Par-1^{T408A}* (Wang et al., 2007), *orbit^{464}*,

g-orbit-tdGFP, *UASp-Orbit^{FL}*, *UASp-GFP-Orbit*, *UASp-Orbit$^{\Delta TOG1}$*, *UASp-Orbit$^{\Delta TOG2}$*, *UASp-Orbit$^{\Delta SxIP}$*, *UASp-Orbit$^{\Delta TOG3}$*, *UASp-Orbit$^{\Delta CLIP\text{-}ID}$*, *UASp-Orbit$^{TOG1,2\text{-}Linker}$*, *UASp-Orbit^{TOG2}*, *UAS-Orbit*, *UAS-Orbit-HA*, *UAS-Orbit-CTAP* (generated in this study).

The following stocks were obtained from Bloomington Stock Center (BSC): *UAS-mCD8::GFP*, *UAS-Dicer2*, *FRT2A*, *tubP-Gal80*, *Gal4$^{109(2)80}$*, *Gal4$^{4-77}$* (BL#8737), *UAS-Nod-β-Gal* (BL#9912), *ppk-CD4-tdGFP* (BL#35843), *GSG2295-Gal4* (BL#40266), *UASp-αTub84B-tdEOS* (BL#51313, 51314), *orbit* RNAi #1 (BL#35442), *CLIP-190* RNAi #1 (BL#31265), *par-1* RNAi #1 (BL#32410), *par-1* RNAi #2 (BL#35342), *par-1-KI-GFP* (BL#64452).

The following stocks were ordered from Vienna *Drosophila* RNAi Center (VDRC): *orbit* RNAi #2 (v108620), control RNAi (v25271), *GCC185* RNAi #1 (v26221), *GCC185* RNAi #2 (v106596), *CLIP-190* RNAi #2 (v107824), *tau* RNAi #1 (v25023), *tau* RNAi #2 (v25024).

S2 cell culture

S2 cells were cultured in Expressive Five SFM (ThermoFisher, 10486025) with 1% L-glutamine at 25°C.

METHOD DETAILS

Generation of *orbit* transgenes

To generate *UAS-Orbit* transgenes, the full-length cDNA of *Drosophila orbit* was amplified from EST LD31673 into *pENTR/D-TOPO* vector (Invitrogen), followed by cloning into the *pTW*, *pPW or pTWH* destination vectors (DGRC) via LR reaction. Various *orbit* truncates were generated by QuickChange mutagenesis kit (Agilent Tech) using *pENTR-orbit* as a template. The *orbit* cDNA was cloned directly into *pUAST-CTAP* plasmid to generate *UAS-Orbit-CTAP* construct.

For the *g-orbit-tdGFP* construct, a tandem dimeric GFP (tdGFP) fragment was first amplified from the *ppk-CD4-tdGFP* flies into *pENTR/D-TOPO* vector to generate *pENTR-tdGFP*. Via homologous recombination (Venken et al., 2009), the tdGFP sequence was then recombined into the BAC clone CH322-62N12 before the stop codon. All the constructs were sent to BestGene Inc for microinjection.

EMS screen, RNAi and MARCM analysis of da neurons

For EMS screen on chromosome 3L, *w*;;FRT2A/FRT2A* male flies were first treated with 25 mM EMS for 1 day to generate random mutations. The mutated chromosomes were balanced over TM6B. The lethal/semi-lethal lines were then isolated for MARCM analysis.

RNAi/MARCM analysis of da neurons were conducted as previously described (Kirilly et al., 2009). Fly embryos were collected every 24 - 48h and kept at 25°C. To check dendrite pruning phenotypes at 16 or 19 h APF, the white prepupae were collected on wet filter paper overnight and pupal cases were carefully removed before mounting with 90% glycerol. To image the full dendritic arbor of ddaC neurons, wandering 3rd instar larvae were washed with water briefly and mounted on the glass slides with a drop of halocarbon oil (Santa Cruze, sc-250077). mCD8::GFP were visualized by Leica SPE-II upright confocal microscope with 40 x oil lens, 1x zoom. Dorsal is up in all images. The imageJ plugin Simple Neurite Tracer and Sholl Analysis were used for dendrite analyses. The dendrite severing defect is defined by the presence of dendrites (at least 100 μm in length) that remain attached to the soma at 16 h APF.

Time-lapse imaging of EB1-GFP

Late 2nd/early 3rd instar larvae (72–96 h AEL) expressing *UAS-EB1-GFP* driven by *Gal4$^{4-77}$* or *ppk-Gal4* were washed with water briefly and mounted with halocarbon oil for time-lapse imaging. EB1-GFP movies were acquired by Olympus FV3000 inverted confocal microscope with 60x oil lens, 3x zoom. Within 3 min, 125 frames of 6-z-step images were obtained at 1.45-s intervals. The kymographs were generated by the ImageJ plugin KymographBuilder.

Microtubule turnover assay

Early/wandering 3rd instar larvae expressing *UASp-αTub84B-EOS* driven by *ppk-Gal4* were washed with water briefly and mounted with halocarbon oil. Green and red EOS images were acquired by Olympus FV3000 inverted confocal microscope with 60x oil lens, 3x zoom. Using a 405 nm laser, EOS in a segment of dorsal proximal dendrite ($\sim$7 μm) was photoconverted from green to red. Using 488 nm and 561 nm lasers, 2 images were acquired just after photoconversion and 30 min after photoconversion. The remaining fluorescence intensity was quantified as (FI[converted] - FI[neighbouring])$_{30min}$/(FI[converted] - FI[neighbouring])$_{0min}$.

RU486/mifepristone treatment

Embryos were collected every 12 h and cultured on normal food. Late 2nd/early 3rd instar larvae were fed with 240 μg/mL RU486 for one day and white pupae were collected for further experimental analyses.

Co-immunoprecipitiation

pAHW-Orbit, *pAMW-Orbit*, *pAFW-GCC185* and *pAWF-Par-1* vectors were generated using Gateway cloning and transfected into S2 cells via Effectene Transfection Reagent (Qiagen, 301427). Transfected S2 cells were homogenized in IP Lysis buffer (Pierce, 87788) with protease inhibitors. The supernatants were used for immunoprecipitation with primary antibodies at 4°C overnight, followed by

incubation with protein A/G beads for 2 h. The beads were then washed with cold PBS for 3 times before standard Western blot analyses.

Immunofluorescence and antibodies

The following antibodies were used in this study: Mouse anti-Futsch (1:50, DSHB, 22C10), mouse anti-α-Tubulin (1:500, Sigma, T9026), Rabbit anti-Tau (1:1000, a gift from Daniel St. Johnston), mouse anti-Galactosidase (1:1000, Promega, Z3781), rabbit anti-GFP (1:1000, Invitrogen, A-11122), rabbit anti-Orbit (1:500, A gift from Claudio E. Sunkel), Cy3-, 488- or 649-conjugated goat secondary antibodies (1:500, Jackson Laboratories).

For normal staining, larvae or pupae from control and experimental groups were dissected simultaneously in cold PBS and fixed with 4% formaldehyde for 20 min. For Futsch staining, the samples were dissected in Ca^{2+} free HL3.1 saline and fixed with PHEM buffer with 0.25% glutaraldehyde, 4% formaldehyde and 0.1% Triton X-100 for 15 min, followed by quenching with 50 mM NH_4Cl for 5 min (Witte et al., 2008). The samples were mounted with VectaShield mounting media and imaged immediately by Olympus FV3000 inverted confocal microscope or Leica SPE-II upright confocal microscope. Multiple z-step images at 1.5 μm interval were taken to include the entire volume of ddaC/E neurons.

For quantification of immunofluorescence data, the mean fluorescence intensity of the cell body (*Par-1-KI-GFP*) of ddaC was measured after subtracting background (Rolling Ball Radius = 50) by ImageJ. The Nod-lacZ/Futsch/HRP intensity in 2 dorsal branches of ddaC/E dendrites (~20 μm in length) that are 30 μm away from the soma were measured and averaged. The fluorescence intensity of each experimental groups was then normalized the average of control group.

QUANTIFICATION AND STATISTICAL ANALYSIS

Two-tailed Student's t-test was used to determine statistical significance for pairwise comparison. One-way ANOVA with Bonferroni test was applied when more than 2 groups were present. The statistical significance was defined as ***$p < 0.001$, **$p < 0.01$, *$p < 0.05$, ns, not significant. Standard error of the mean (SEM) was presented in the error bars of all graphs. The number of samples (n) equals the number of neurons. All data are from at least 3 biological repeats.

Cell Reports, Volume *39*

Supplemental information

Drosophila CLASP regulates microtubule orientation and dendrite pruning by suppressing Par-1 kinase

Shufeng Bu, Quan Tang, Yan Wang, Samuel Song Yuan Lau, Wei Lin Yong, and Fengwei Yu

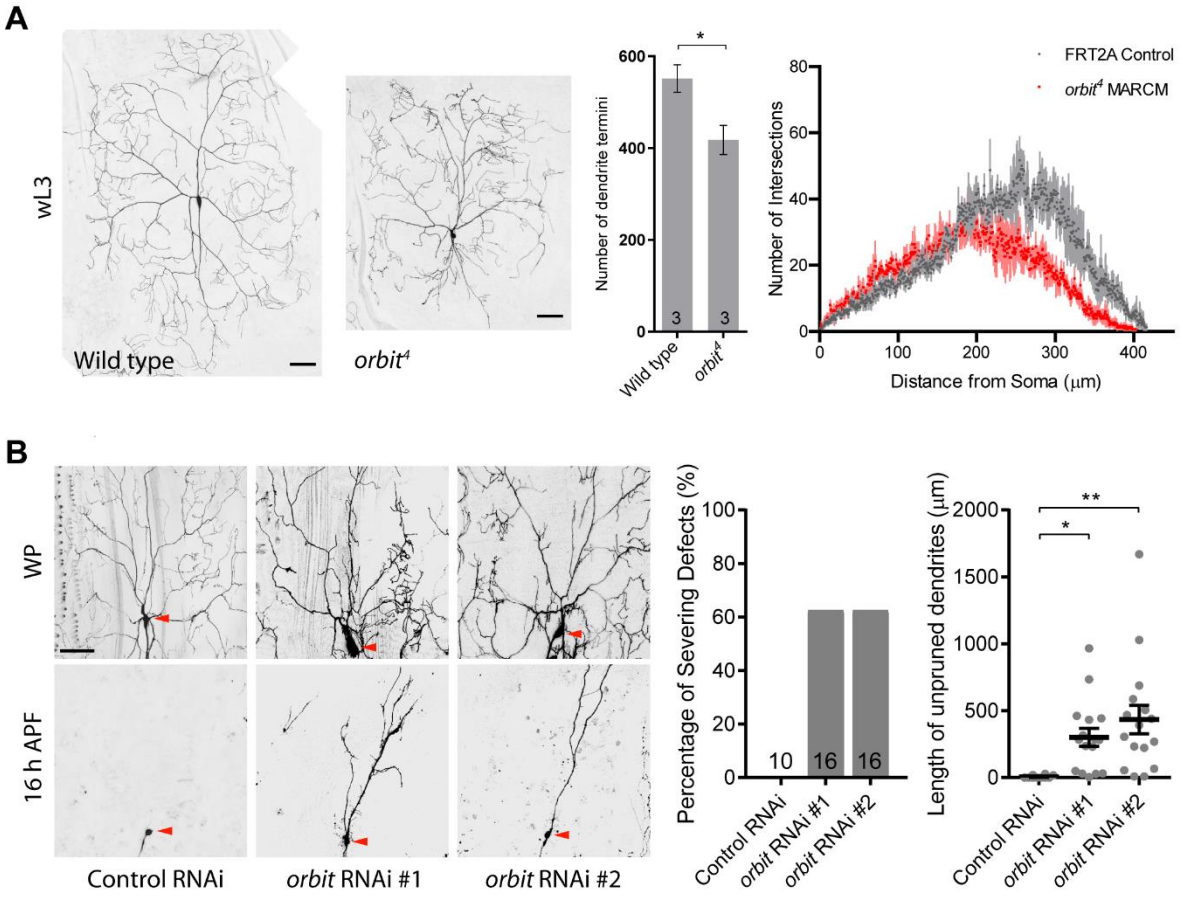
A
wL3
Wild type
orbit4
Number of dendrite termini
600
400
200
0
3
3
Wild type
orbit4
*
FRT2A Control
orbit4 MARCM
Number of Intersections
80
60
40
20
0
0
100
200
300
400
Distance from Soma (μm)
B
WP
16 h APF
Control RNAi
orbit RNAi #1
orbit RNAi #2
Percentage of Severing Defects (%)
100
80
60
40
20
0
10
16
16
Control RNAi
orbit RNAi #1
orbit RNAi #2
Length of unpruned dendrites (μm)
2000
1500
1000
500
0
*
**
Control RNAi
orbit RNAi #1
orbit RNAi #2
C
g-Orbit-tdGFP / α-Tubulin
Orbit-tdGFP
α-Tubulin
g-Orbit-tdGFP / α-Tubulin
Orbit-tdGFP
α-Tubulin
D
ppk-Gal4 > UASp-GFP-Orbit / α-Tubulin
GFP-Orbit
α-Tubulin
A58-Gal4 > UASp-GFP-Orbit / α-Tubulin
GFP-Orbit
α-Tubulin

Figure S1. Orbit is endogenously expressed in ddaC neurons and co-localizes with α-tubulin on the microtubule lattices. Related to Figure 1 and Table S1.

(A) Dendrites of wild type and *orbit*^{4} mutant ddaC neurons at wL3 stage (Biological Replicates = 3). Quantification of dendrite termini numbers and sholl analysis. **(B)** Dendrites of ddaC neurons expressing control RNAi, *orbit* RNAi #1 and #2 at WP and 16 h APF. Red arrowheads point to the ddaC soma (Biological Replicates = 3). Quantitative analyses of dendrite severing defects and unpruned dendrite lengths. **(C)** Endogenous expression of *g-Orbit-tdGFP* in the da sensory neurons (left) and the surrounding epidermal cells (right) co-stained with GFP (green) and α-tubulin (magenta). Arrowheads point to the dendrites and asterisks label the somas of ddaC neuron (Biological Replicates = 4). **(D)** Expression of *UASp-GFP-Orbit* driven by *ppk-Gal4* in ddaC neurons (left) and *A58-Gal4* in epidermal cells (right) co-stained with GFP (green) and α-tubulin (magenta). Arrowheads point to the dendrites and asterisks label the somas of ddaC neuron (Biological Replicates = 4). The error bars represent SEM. The scale bars in **(A, B)** and **(C, D)** represent 50 μm and 10 μm, respectively. *$p<0.05$, **$p<0.01$.

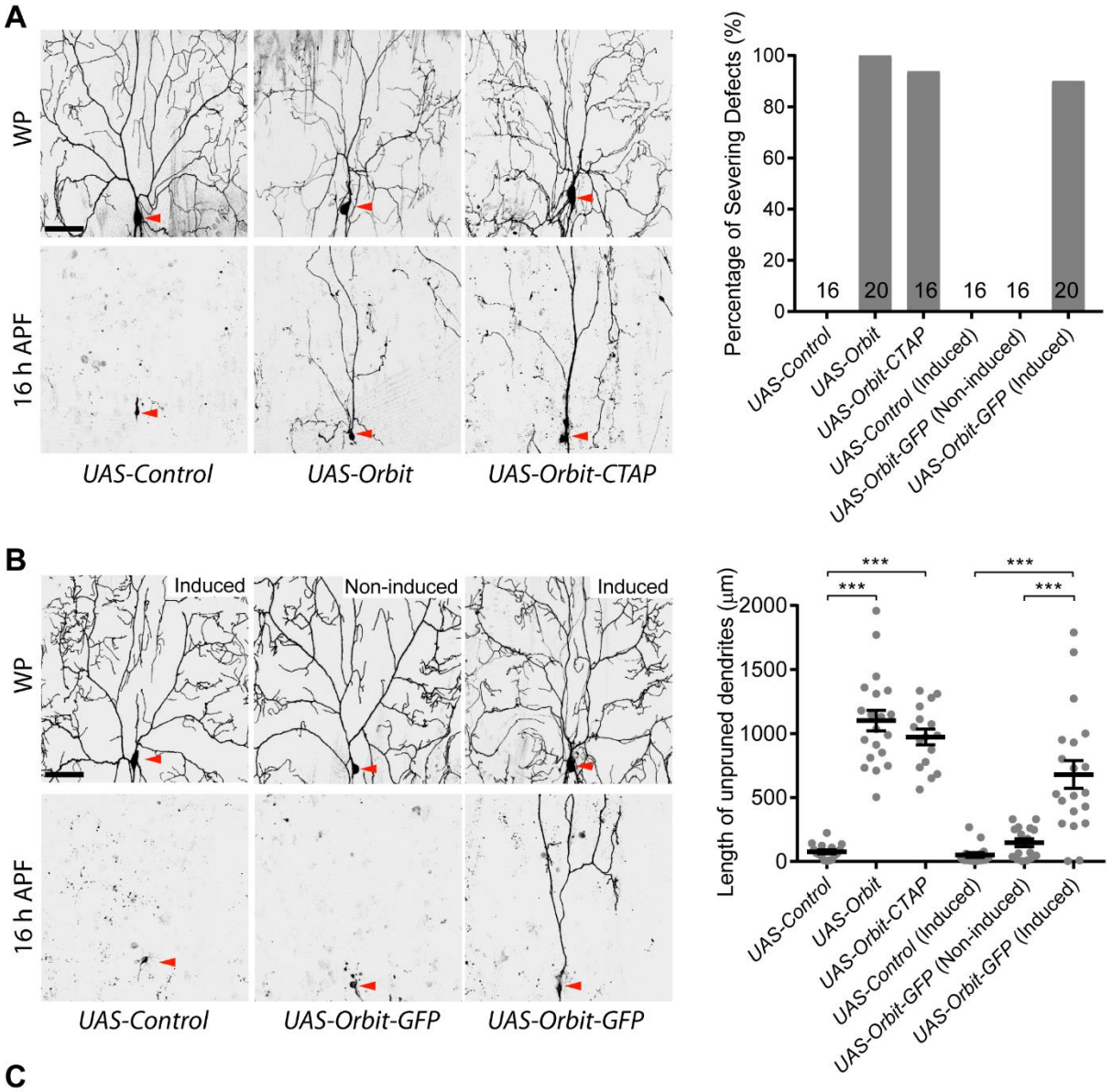
A
WP
16 h APF
UAS-Control
UAS-Orbit
UAS-Orbit-CTAP
Percentage of Severing Defects (%)
100
80
60
40
20
0
16
20
16
16
16
20
UAS-Control
UAS-Orbit
UAS-Orbit-CTAP
UAS-Control (Induced)
UAS-Orbit-GFP (Non-induced)
UAS-Orbit-GFP (Induced)
B
Induced
Non-induced
Induced
WP
16 h APF
UAS-Control
UAS-Orbit-GFP
UAS-Orbit-GFP
Length of unpruned dendrites (µm)
2000
1500
1000
500
0
***
***
***
***
UAS-Control
UAS-Orbit
UAS-Orbit-CTAP
UAS-Control (Induced)
UAS-Orbit-GFP (Non-induced)
UAS-Orbit-GFP (Induced)
C
anti-Orbit
GFP / anti-Orbit
UAS-Control
UASp-Orbit
UASt-Orbit
UASt-Orbit-HA

Figure S2. Overexpression of Orbit inhibits dendrite pruning in ddaC neurons. Related to Figure 1 and Table S1.

(A) Dendrites of ddaC neurons continuously expressing *UAS-Control*, *UAS-Orbit* and *UAS-Orbit-CTAP* at WP and 16 h APF. Red arrowheads point to the soma of ddaC. Quantitative analyses of dendrite severing defects and unpruned dendrite length at 16 h APF (Biological Replicates = 4). **(B)** Dendrites of ddaC neurons expressing *UAS-Control* and *UAS-Orbit-GFP* under control of *Geneswitch-Gal4* at WP and 16 h APF. Red arrowheads point to the soma of ddaC (Biological Replicates = 4). Quantitative analyses of dendrite severing defects and unpruned dendrite length at 16 h APF. **(C)** Confocal images of ddaC neurons (green) expressing *UAS-Control*, *UASp-Orbit*, *UASt-Orbit* and *UASt-Orbit-HA* and immunostained with anti-Orbit (magenta). The ddaC soma is marked by dashed lines (Biological Replicates = 4). The error bars represent SEM. The scale bars in **(A, B)** and **(C)** represent 50 µm and 10 µm, respectively. ***p<0.001.

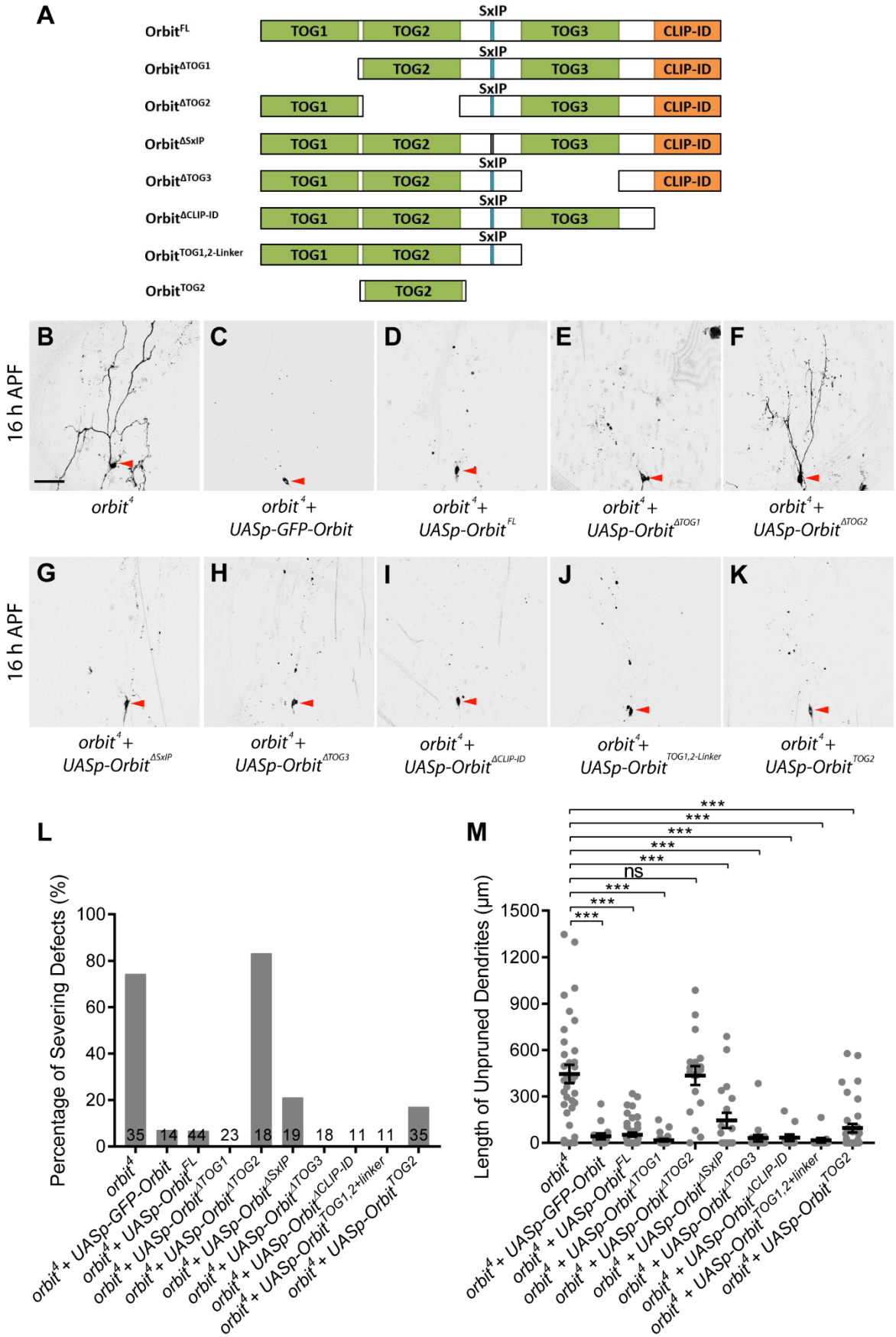
A
Orbit^FL
Orbit^ΔTOG1
Orbit^ΔTOG2
Orbit^ΔSxIP
Orbit^ΔTOG3
Orbit^ΔCLIP-ID
Orbit^TOG1,2-Linker
Orbit^TOG2
SxIP
TOG1
TOG2
TOG3
CLIP-ID
16 h APF
B
C
D
E
F
orbit^4
orbit^4+ UASp-GFP-Orbit
orbit^4+ UASp-Orbit^FL
orbit^4+ UASp-Orbit^ΔTOG1
orbit^4+ UASp-Orbit^ΔTOG2
G
H
I
J
K
orbit^4+ UASp-Orbit^ΔSxIP
orbit^4+ UASp-Orbit^ΔTOG3
orbit^4+ UASp-Orbit^ΔCLIP-ID
orbit^4+ UASp-Orbit^TOG1,2-Linker
orbit^4+ UASp-Orbit^TOG2
L
Percentage of Severing Defects (%)
100
80
60
40
20
0
35
14
44
23
18
19
18
11
11
35
M
Length of Unpruned Dendrites (µm)
1500
1200
900
600
300
0
***
ns

Figure S3. The TOG2 domain is required for Orbit to regulate dendrite pruning. Related to Figure 1 and Table S1.

(A) A diagram of *Drosophila* Orbit protein structure and a series of truncated proteins used for rescue experiments. **(B-K)** Dendrites of ddaC neurons expressing *UASp-GFP-Orbit* **(C)**, *UASp-Orbit*^{FL} **(D)**, *UASp-Orbit*$^{\Delta TOG1}$ **(E)**, *UASp-Orbit*$^{\Delta TOG2}$ **(F)**, *UASp-Orbit*$^{\Delta SxIP}$ **(G)**, *UASp-Orbit*$^{\Delta TOG3}$ **(H)**, *UASp-Orbit*$^{\Delta CLIP\text{-}ID}$ **(I)**, *UASp-Orbit*$^{TOG1,2\text{-}Linker}$ **(J)** and *UASp-Orbit*^{TOG2} **(K)**, under *orbit*^{4} mutant background **(B)** at 16 h APF. Red arrowheads point to the soma of ddaC. **(L-M)** Quantitative analyses of dendrite severing defects and unpruned dendrite length at 16 h APF (Biological Replicates > 5). The error bars represent SEM. The scale bar in **(B)** represents 50 μm. ns, not significant, ***p<0.001.

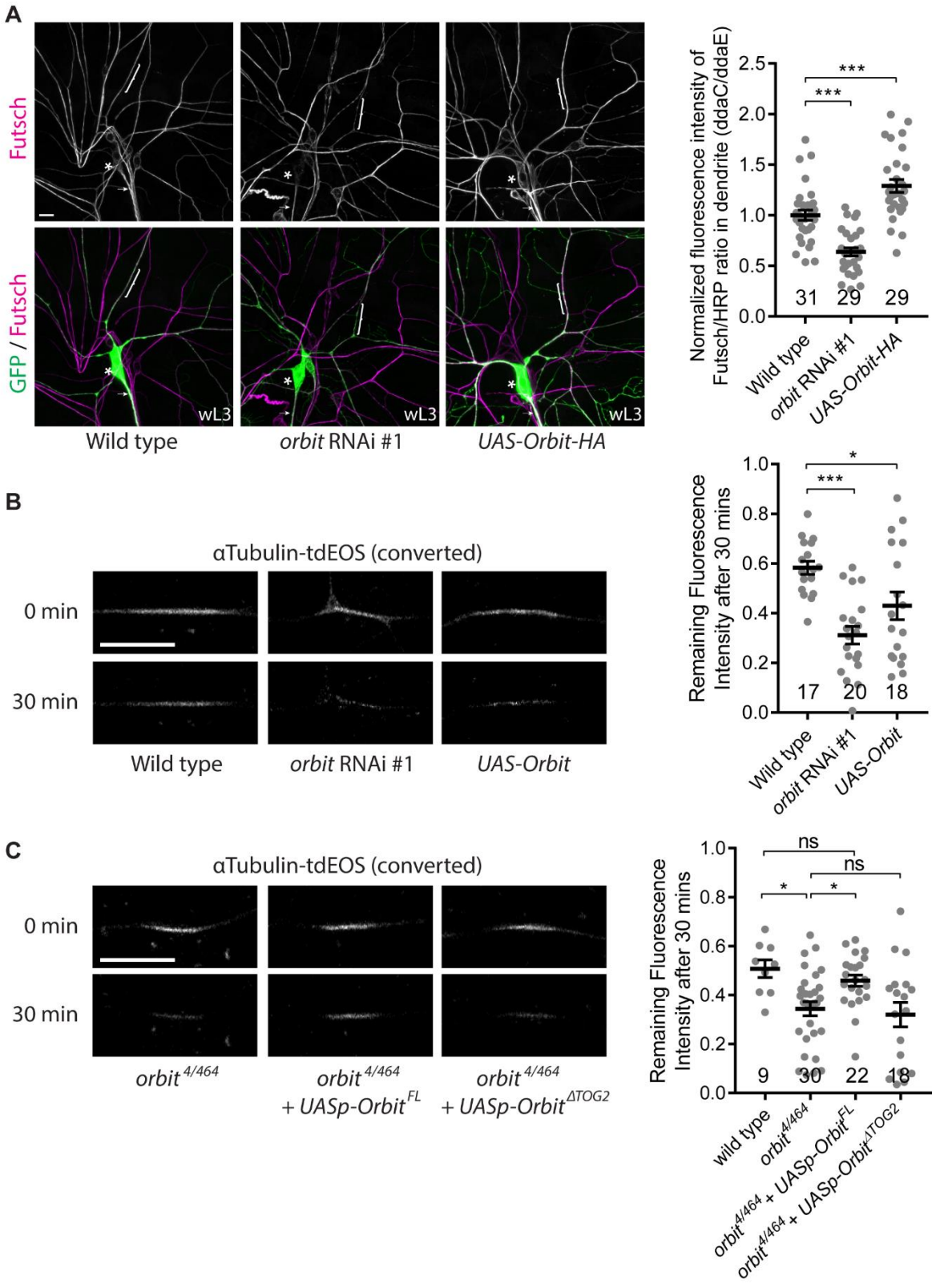
A
Futsch
GFP / Futsch
wL3
wL3
wL3
Wild type
orbit RNAi #1
UAS-Orbit-HA
Normalized fluorescence intensity of Futsch/HRP ratio in dendrite (ddaC/ddaE)
2.5
2.0
1.5
1.0
0.5
0.0
***
***
31
29
29
Wild type
orbit RNAi #1
UAS-Orbit-HA
B
αTubulin-tdEOS (converted)
0 min
30 min
Wild type
orbit RNAi #1
UAS-Orbit
Remaining Fluorescence Intensity after 30 mins
1.0
0.8
0.6
0.4
0.2
0.0
*
***
17
20
18
Wild type
orbit RNAi #1
UAS-Orbit
C
αTubulin-tdEOS (converted)
0 min
30 min
orbit 4/464
orbit 4/464 + UASp-Orbit FL
orbit 4/464 + UASp-Orbit ΔTOG2
Remaining Fluorescence Intensity after 30 mins
1.0
0.8
0.6
0.4
0.2
0.0
ns
ns
*
*
9
30
22
18
wild type
orbit 4/464
orbit 4/464 + UASp-Orbit FL
orbit 4/464 + UASp-Orbit ΔTOG2

Figure S4. Orbit regulates dendritic microtubule stability and turnover in the dendrites of ddaC neurons. Related to Figure 2 and Table S1.

(A) Microtubule/Futsch (magenta) levels in ddaC neurons (green) of wild type, *orbit* RNAi #1 and Orbit-HA overexpression at wL3 stage. The asterisks label the ddaC somas, the arrows point to the axons and the brackets mark the dendrites. Quantitative analysis of microtubule levels in the ddaC dendrites (Biological Replicates > 5). **(B)** Microtubule turnover assay in ddaC neurons of wild type, *orbit* RNAi #1 or Orbit-HA overexpression at wL3 stage (Biological Replicates > 3). The photo-converted tdEOS::α-Tubulin signal at 0 min and after 30 min is shown in the left panel. Quantitative analysis of microtubule turnover rate in the ddaC dendrites as indicated by the remaining fluorescence intensity of converted EOS after 30 min is in the right panel. **(C)** Microtubule turnover assay in $orbit^{4/464}$ mutant ddaC neurons expressing $UASp\text{-}Orbit^{FL}$ or $UASp\text{-}Orbit^{\Delta TOG2}$ at wL3 stage (Biological Replicates > 3). The photo-converted tdEOS::α-Tubulin signal at 0 min and after 30 min is shown in the left panel. Remaining fluorescence intensity of converted EOS after 30 min is in the right panel. The error bars represent SEM. The scale bars in **(A-C)** represent 10 µm. ns, not significant, *p<0.05, ***p<0.001.

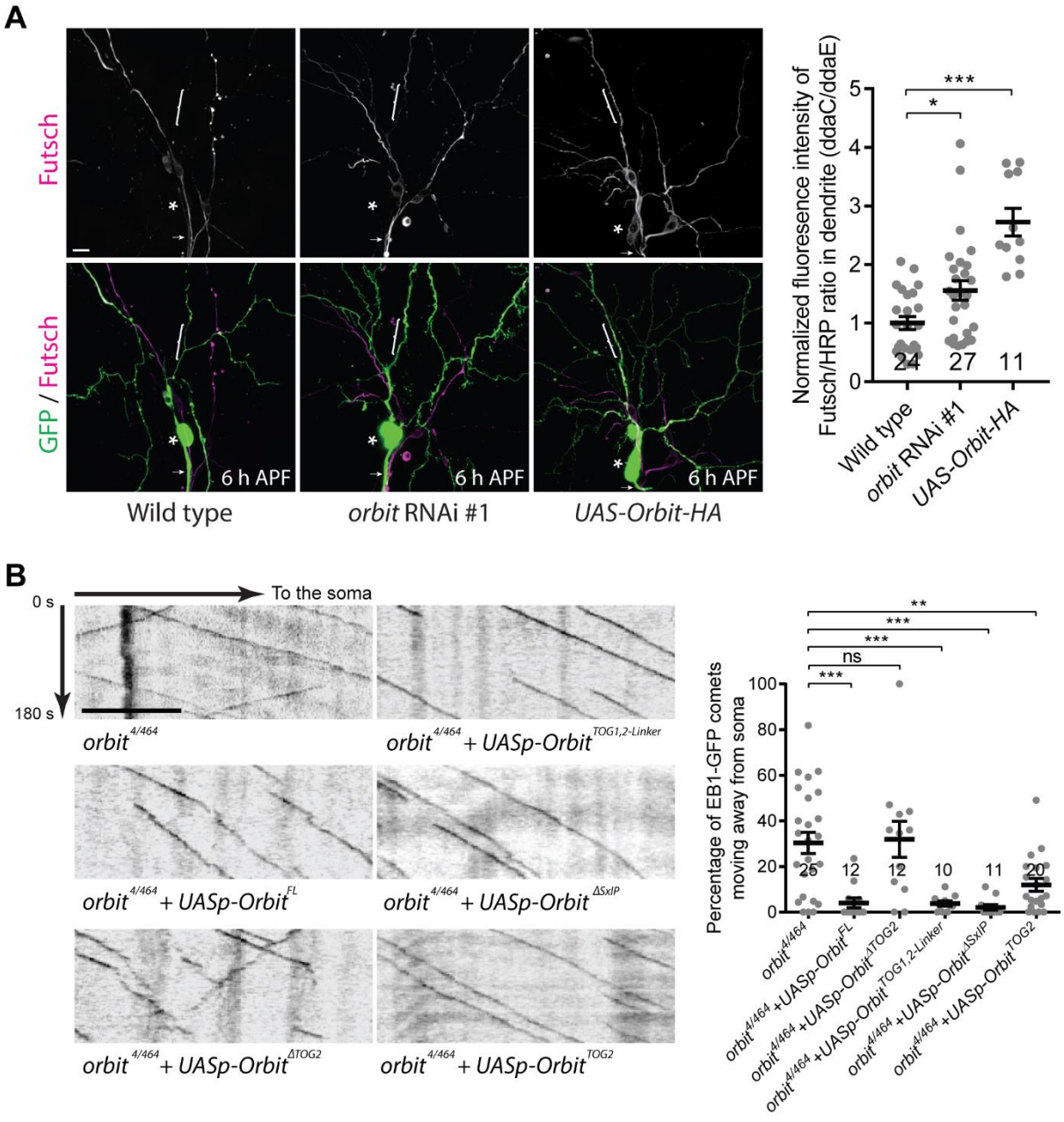
A
Futsch
GFP / Futsch
6 h APF
Wild type
orbit RNAi #1
UAS-Orbit-HA
Normalized fluoresence intensity of Futsch/HRP ratio in dendrite (ddaC/ddaE)
24
27
11
B
0 s
180 s
To the soma
orbit4/464
orbit4/464 + UASp-OrbitTOG1,2-Linker
orbit4/464 + UASp-OrbitFL
orbit4/464 + UASp-OrbitΔSxIP
orbit4/464 + UASp-OrbitΔTOG2
orbit4/464 + UASp-OrbitTOG2
Percentage of EB1-GFP comets moving away from soma
ns
25
12
12
10
11
20
C
Input
IP: Flag
IP: Myc
Flag-GCC185
Myc-Orbit
IB: Flag
IB: Myc
150 KD
150 KD

Figure S5. Both knockdown and overexpression of Orbit lead to elevated microtubule levels in the dendrites prior to dendrite pruning. Related to Figure 2 and Table S1.

(A) Microtubule/Futsch (magenta) levels in ddaC neurons (green) of wild type, *orbit* RNAi #1 or overexpressing Orbit-HA at 6 h APF. The asterisks label the ddaC somas, the arrows point to the axons and the brackets mark the dendrites (Biological Replicates = 5). Quantitative analysis of microtubule levels in the ddaC dendrites. **(B)** Dendritic EB1-GFP kymographs in $orbit^{4/464}$ mutant ddaC neurons expressing $UASp\text{-}Orbit^{FL}$, $UASp\text{-}Orbit^{\Delta TOG2}$, $UASp\text{-}Orbit^{TOG1,2\text{-}Linker}$, $UASp\text{-}Orbit^{\Delta SxIP}$ or $UASp\text{-}Orbit^{TOG2}$ (Biological Replicates > 3). Quantitative analysis of EB1-GFP orientation in the ddaC dendrites. **(C)** Co-immunoprecipitation of Flag-GCC185 and Myc-Orbit in *Drosophila* S2 cells. 3% inputs were blotted with anti-Flag or anti-Myc antibodies. GCC185 and Orbit does not interact with each other in S2 cells (Biological Replicates = 3). The error bars represent SEM. The scale bars in **(A, B)** represent 10 µm. ns, not significant, *p<0.05, ***p<0.001.

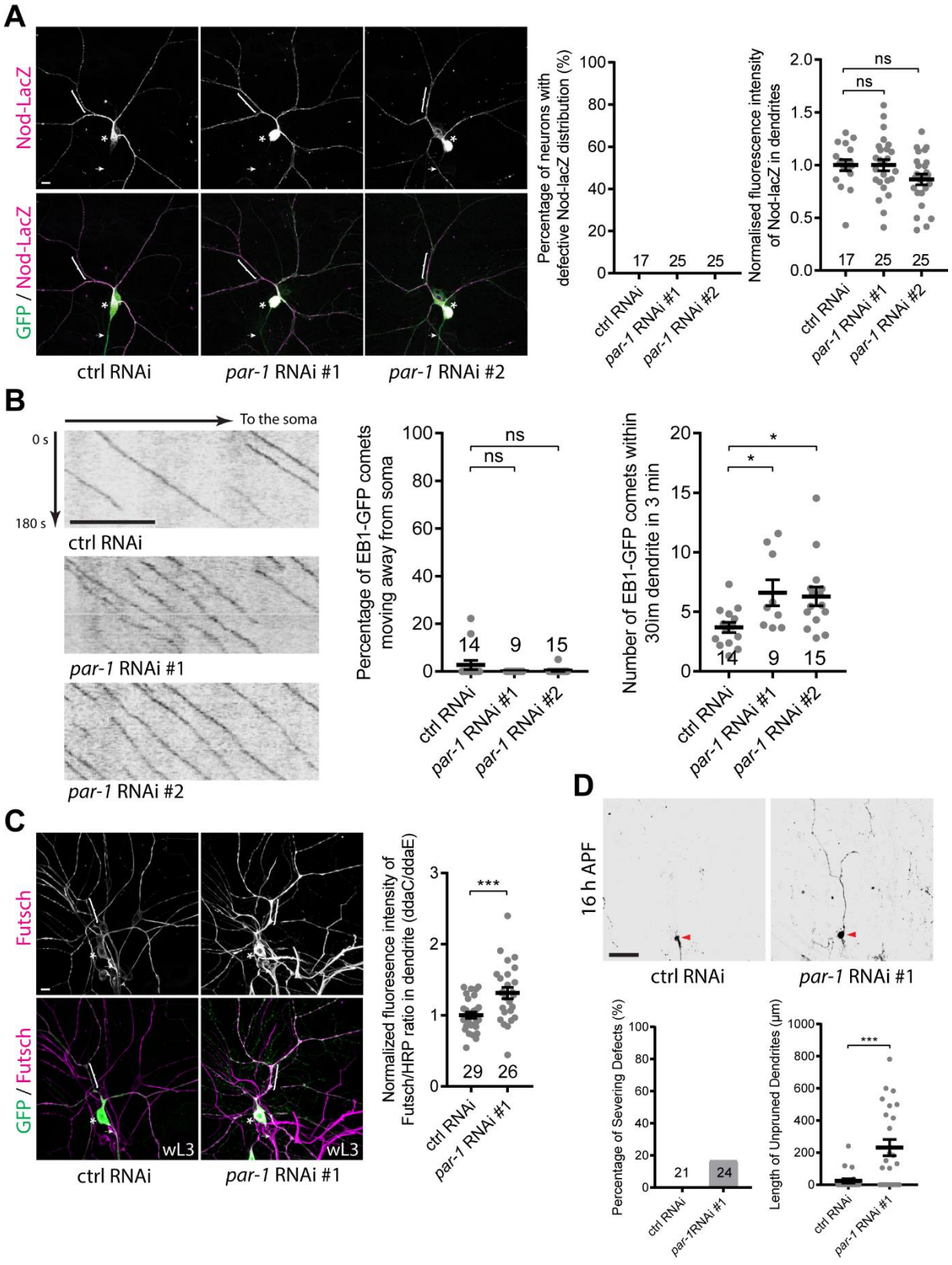
A
Nod-LacZ
GFP / Nod-LacZ
ctrl RNAi
par-1 RNAi #1
par-1 RNAi #2
Percentage of neurons with defective Nod-lacZ distribution (%)
17 25 25
Normalised fluorescence intensity of Nod-lacZ in dendrites
ns
ns
17 25 25
B
To the soma
0 s
180 s
ctrl RNAi
par-1 RNAi #1
par-1 RNAi #2
Percentage of EB1-GFP comets moving away from soma
ns
ns
14 9 15
Number of EB1-GFP comets within 30im dendrite in 3 min
*
*
14 9 15
C
Futsch
GFP / Futsch
wL3
wL3
ctrl RNAi
par-1 RNAi #1
Normalized fluorescence intensity of Futsch/HRP ratio in dendrite (ddaC/ddaE)
***
29 26
D
16 h APF
ctrl RNAi
par-1 RNAi #1
Percentage of Severing Defects (%)
21 24
Length of Unpruned Dendrites (µm)
***

Figure S6. Par-1 negatively regulates microtubule/Futsch levels in the dendrites and is dispensable for the dendritic minus-end-out microtubule orientation. Related to Figure 3 and Table S1.

(A) Expression of Nod-lacZ (magenta) in ddaC neurons (green) expressing ctrl RNAi, *par-1* RNAi #1 or #2. The asterisks label the ddaC somas, the arrows point to the axons and the brackets mark the dendrites (Biological Replicates = 5). Quantitative analyses of Nod-lacZ distribution in ddaC neurons. **(B)** Dendritic EB1-GFP kymographs in ddaC neurons expressing ctrl RNAi, *par-1* RNAi #1 or #2 (Biological Replicates > 3). Quantitative analysis of EB1-GFP orientation and number. **(C)** Microtubule/Futsch (magenta) levels in ddaC neurons (green) of ctrl RNAi and *par-1* RNAi #1 at wL3 stage. The asterisks label the ddaC somas, the arrows point to the axons and the brackets mark the dendrites (Biological Replicates > 5). Quantitative analysis of microtubule levels in the ddaC dendrites. **(D)** Dendrites of ddaC neurons expressing ctrl RNAi and *par-1* RNAi #1 at 16 h APF. Red arrowheads point to the soma of ddaC. Quantitative analyses of dendrite severing defects and unpruned dendrite length (Biological Replicates > 5). The error bars represent SEM. The scale bars in **(A-C)** and **(D)** represent 10 μm and 50 μm, respectively. ns, not significant, *$p<0.05$, ***$p<0.001$.

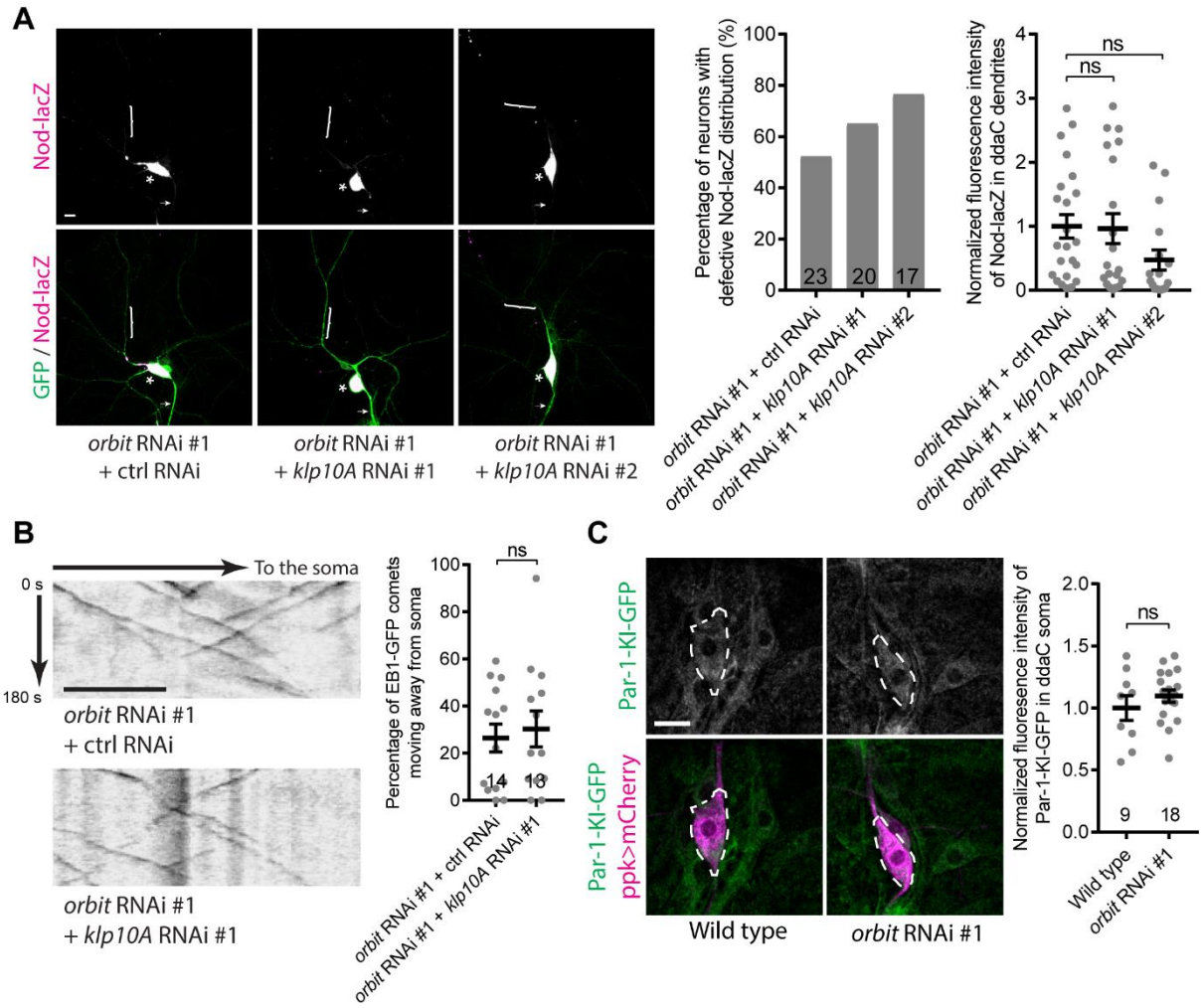
A
Nod-lacZ
GFP / Nod-lacZ
orbit RNAi #1 + ctrl RNAi
orbit RNAi #1 + klp10A RNAi #1
orbit RNAi #1 + klp10A RNAi #2
Percentage of neurons with defective Nod-lacZ distribution (%)
23
20
17
Normalized fluorescence intensity of Nod-lacZ in ddaC dendrites
ns
ns
B
To the soma
0 s
180 s
orbit RNAi #1 + ctrl RNAi
orbit RNAi #1 + klp10A RNAi #1
Percentage of EB1-GFP comets moving away from soma
14
18
ns
C
Par-1-KI-GFP
Par-1-KI-GFP ppk>mCherry
Wild type
orbit RNAi #1
Normalized fluoresence intensity of Par-1-KI-GFP in ddaC soma
9
18
ns
Wild type
orbit RNAi #1
D
Input
IP: Flag
IP: Myc
Flag-Par-1
Myc-Orbit
IB: Flag
IB: Myc
150 KD
150 KD

Figure S7. Knockdown of Klp10A did not rescue the microtubule orientation defects in the dendrites of *orbit* RNAi neurons. Related to Figure 3 and Table S1.

(A) Expression of Nod-lacZ (magenta) in *orbit* RNAi #1 ddaC neurons (green) co-expressing ctrl RNAi, *klp10A* RNAi #1 or #2 construct. The asterisks label the ddaC somas, the arrows point to the axons and the brackets mark the dendrites (Biological Replicates = 5). Quantitative analysis of Nod-lacZ distribution in the ddaC dendrites. **(B)** Dendritic EB1-GFP kymographs in *orbit* RNAi #1 + ctrl RNAi and *orbit* RNAi #1 + *klp10A* RNAi #1 ddaC neurons. The horizontal arrow marks the direction toward the soma. The vertical arrow indicates the duration (Biological Replicates > 3). Quantitative analysis of EB1-GFP orientation in the dendrites. **(C)** Endogenous expression of *Par-1-KI-GFP* (green) in wild-type and *orbit* RNAi #1 ddaC neurons (magenta) (Biological Replicates = 3). Quantification of *Par-1-KI-GFP* levels in the ddaC soma. The ddaC soma is marked by dashed lines. **(D)** Co-immunoprecipitation of Par-1-Flag and Myc-Orbit in transfected S2 cells. 3% inputs were blotted with anti-Flag or anti-Myc antibodies. Par-1 and Orbit does not interact with each other in S2 cells (Biological Replicates = 3). The error bars represent SEM. The scale bars in **(A, B)** represent 10 μm. ns, not significant.

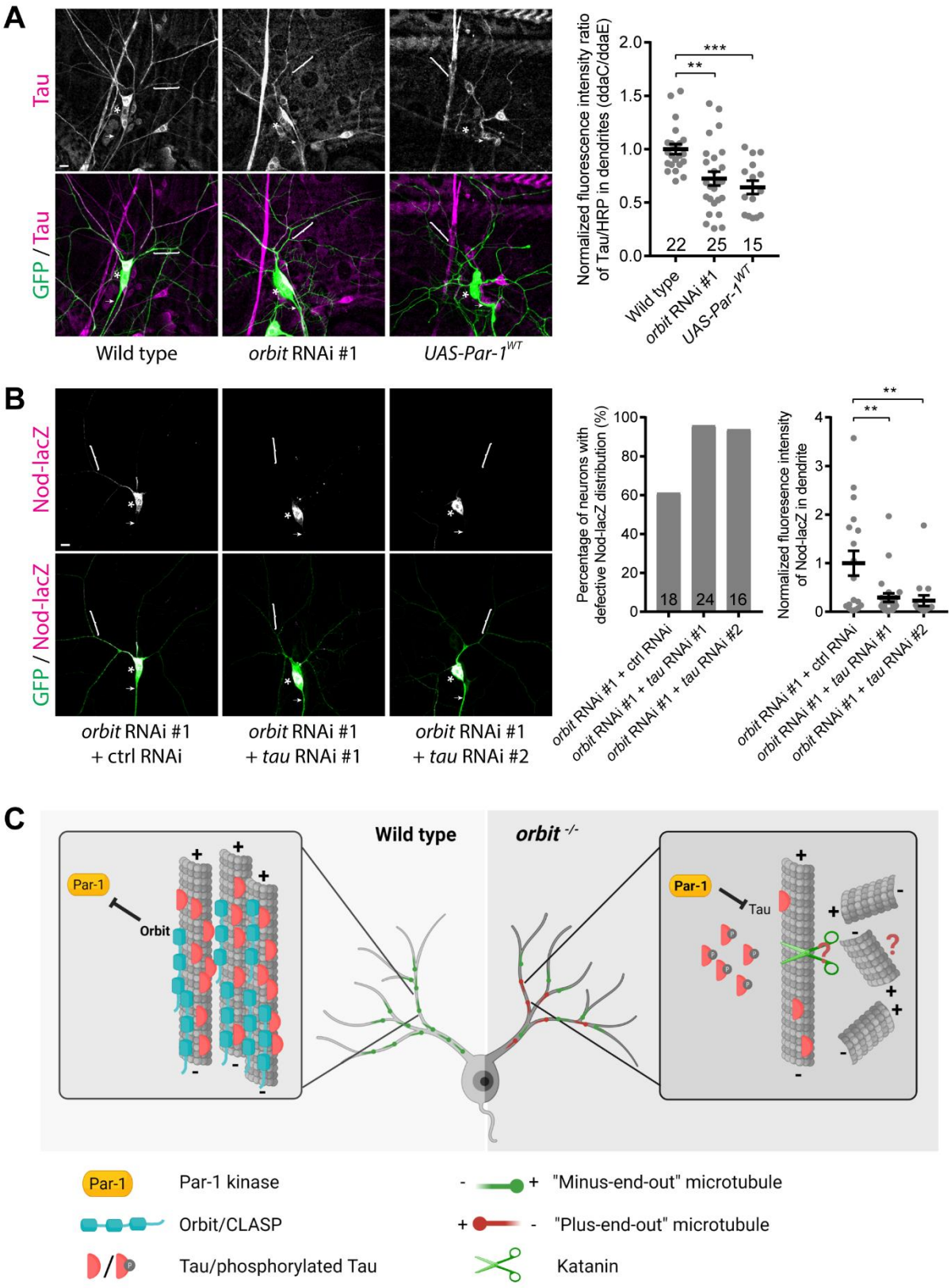
A
Tau
GFP / Tau
Wild type
orbit RNAi #1
UAS-Par-1WT
Normalized fluorescence intensity ratio of Tau/HRP in dendrites (ddaC/ddaE)
2.0
1.5
1.0
0.5
0.0
***
**
22
25
15
Wild type
orbit RNAi #1
UAS-Par-1WT
B
Nod-lacZ
GFP / Nod-lacZ
orbit RNAi #1 + ctrl RNAi
orbit RNAi #1 + tau RNAi #1
orbit RNAi #1 + tau RNAi #2
Percentage of neurons with defective Nod-lacZ distribution (%)
100
80
60
40
20
0
18
24
16
Normalized fluoresence intensity of Nod-lacZ in dendrite
4
3
2
1
0
**
**
C
Wild type
orbit -/-
Par-1
Orbit
Tau
Par-1 kinase
Orbit/CLASP
Tau/phosphorylated Tau
"Minus-end-out" microtubule
"Plus-end-out" microtubule
Katanin

Figure S8. Tau attenuation exacerbates the Nod-LacZ defect in *orbit* RNAi neurons. Related to Figure 4 and Table S1.

(A) Tau (magenta) expression levels in the dendrites of wild type, *orbit* RNAi #1 and Par-1^{WT}-overexpressing ddaC neurons (green) at wL3 stage. The asterisks label the ddaC somas, the arrows point to the axons and the brackets mark the dendrites (Biological Replicates = 5). Quantitative analysis of Tau levels in the ddaC dendrites. **(B)** Expression of Nod-lacZ (magenta) in *orbit* RNAi #1 ddaC neurons (green) co-expressing ctrl RNAi, *tau* RNAi #1 or #2 constructs. The asterisks label the ddaC somas, the arrows point to the axons and the brackets mark the dendrites (Biological Replicates = 4). Quantitative analysis of Nod-lacZ distribution in the ddaC dendrites. **(C)** A potential model. Orbit acts on microtubule lattices to protect microtubules and maintain dendritic microtubule orientation by suppressing Par-1 function. The error bars represent SEM. The scale bars in **(A, B)** represent 10 µm. **p<0.01, ***p<0.001.